# Grain Refinement of Alloys in Fusion-Based Additive Manufacturing Processes

DUYAO ZHANG, ARVIND PRASAD, MICHAEL J. BERMINGHAM, CARMELO J. TODARO, MICHAEL J. BENOIT, MITESH N. PATEL, DONG QIU, DAVID H. STJOHN, MA QIAN, and MARK A. EASTON

One of the less desirable aspects of fusion-based additive manufacturing is the propensity for coarse columnar grain structures crossing build layers to form. This paper initially attempts to explain the reason for the formation of columnar grain structures in terms of the high thermal gradients typically observed during solidification and the alloy compositions that are typically used which promote epitaxial growth. Successful approaches to the grain refinement of titanium alloys using alloying elements that produce constitutional supercooling are discussed along with the difficulty with nucleant additions. Much of the grain-refining technology already used in aluminium casting is shown to also be applicable to additive manufacturing, although the novelty of the effective use of nanoparticles as nucleants is highlighted. It is also shown that for other alloy systems for which there is a lack of grain-refining technology using chemical means, mechanical means, such as ultrasonic treatment, can be effective across a wide range of alloys. Finally, consideration is given to the difficulties and the possible solutions of producing parts layer by layer. In particular, the importance of understanding nucleation in solidification conditions characterized by high cooling rates and thermal gradients; the importance of melt dynamics; and how previous layers could provide possibilities for refinement of the subsequent layer are highlighted.

https://doi.org/10.1007/s11661-020-05880-4


## I. INTRODUCTION

METAL fusion additive manufacturing (AM) is currently revolutionizing manufacturing across multiple industries, particularly for aerospace, automotive, and biomedical applications. While metal AM offers greater design flexibility and shorter lead times and enables a higher level of product customization similar to that of polymer-based AM processes, metal AM has additional challenges, one of which is controlling the grain structure during solidification.[1] Despite the process variations associated with metal AM (*e.g.*, feed material: wire/powder; power source: laser/electron beam/electric arc), the solidification process shares several common features, *i.e.*, high thermal gradient ($G$), high cooling rate, and complex thermal cycles that can induce partial re-melting of the deposited materials. A high thermal gradient and a high cooling rate usually result in epitaxial growth, and local re-melting of the previously deposited material can eliminate the potential equiaxed grains that have formed in the top part of melt pool. Accordingly, columnar grains are frequently observed in as-fabricated components, which may suffer from hot tearing, solute segregation, and anisotropic mechanical properties.[2] It is not straightforward and often not practical to alter the grain structure of the AM component by thermo-mechanical processing, hence the best solution is to promote the formation of fine, equiaxed grains during solidification.

It is well recognized that the columnar to equiaxed transition (CET) occurs during the initial transient stage of solidification when potent nucleants are present in the melt, and the amount of constitutional supercooling ($\Delta T_{CS}$) exceeds the critical undercooling for nucleation ($\Delta T_n$).[3] The concept of constitutional supercooling (CS) was first applied to CET by Winegard and

DUYAO ZHANG, CARMELO J. TODARO, MICHAEL J. BENOIT, MITESH N. PATEL, DONG QIU, MA QIAN, and MARK A. EASTON are with the Centre for Additive Manufacturing, School of Engineering, RMIT University, Melbourne, 3000, Australia. Contact e-mail: mark.easton@rmit.edu.au ARVIND PRASAD, MICHAEL J. BERMINGHAM, and DAVID H. STJOHN are with the Centre for Advanced Materials Processing and Manufacturing, School of Mechanical and Mining Engineering, University of Queensland, Queensland, 4000, Australia.

Manuscript submitted January 17, 2020.
Article published online June 25, 2020

Chalmers in 1954.[4] The CET can be promoted by adding solute and/or inoculants and controlling the solidification parameters. Effective solute usually has a high growth restriction factor ($Q$) equal to $mC_0(k-1)$, where $m$ is the slope of the liquidus line, $C_0$ is the solute concentration in the bulk alloy, and $k$ is the partition coefficient. Along with the effect of solute, the number density of activated nucleant particles determines the grain morphology and the grain size. A well-established CS zone is an essential condition to activate the potent nucleant particles and trigger waves of heterogeneous nucleation ahead of the solidification front. A larger $Q$-value enables more rapid development of the CS zone ahead of the solidification front.[5] Nucleation occurs in the CS zone when potent nucleant particles (*i.e.*, low $\Delta T_n$) are present, which usually have excellent crystallographic matching with the host metal matrix.[6] It is also worth mentioning that the difference in solidification conditions between conventional casting and metal AM will affect the role of solute and inoculants when triggering a heterogeneous nucleation event. The solidification conditions during AM and the role of variables in understanding grain refinement in AM will be elaborated in Section II.

CET models have been developed and refined over the past decades. For example, Hunt[7] developed an analytical dendritic growth model based on the potential for equiaxed grains to nucleate in the CS zone ahead of the columnar front in order to predict the CET. Then, Gäumann *et al.*[8] added non-equilibrium effects to Hunt's model and extended its application to rapid solidification. Further developments of CET models incorporate the nucleation-free zone (NFZ), which is a region generated by CS in front of the solid/liquid ($S/L$) interface that has insufficient supercooling for nucleation to occur. Thus, a key strategy for grain refinement is to reduce the size of the NFZ, which has been recognized by St John *et al.*[3] Ma *et al.*[9], Shu *et al.*[10], and Du and Li.[11]

Several models have been developed to determine the potency of the nucleant particles. The free growth model[12] developed by Greer *et al.* is commonly used to determine the potency of particles.[13–15] Zhang *et al.* further considered the importance of crystallographic matching by applying their edge-to-edge matching model to explain the effectiveness of grain refiners and have successfully applied this to Al and Mg alloys.[6,16–18] More recently, Fan *et al.*[19] explained the growth of grains by elucidating the mechanisms of heterogeneous nucleation by epitaxial growth from substrates. St John *et al.*[3] developed the Interdependence Model to predict the possibility of nucleation events occurring while the pre-existing grain grows, by considering the effects of inoculating particles and solute in one relationship. The grain size $d_{gs}$ can be expressed as

$$d_{gs} = x_{cs} + x_{dl} + x_{sd}, \qquad [1]$$

where $x_{cs}$ is the amount of growth of a grain to generate CS, $x_{dl}$ is the distance in front of the $S/L$ interface to the maximum CS, and $x_{sd}$ is the average distance between the end of the diffusion field and the next most potent (largest) particle in the melt. Typically, the NFZ is characterized as the sum of $x_{cs} + x_{dl}$. Furthermore, it has been shown,

$$d_{gs} = \frac{Dz\Delta T_n}{vQ} + \frac{4.6D}{v}\left(\frac{C_l^* - C_0}{C_l^*(1-k)}\right) + x_{sd}, \qquad [2]$$

where $D$ is the diffusion rate of the solute in the liquid, $z$ is the proportion of CS that needs to be regenerated after each nucleation event to trigger the next event, $v$ the initial growth velocity, and $C_l^*$ is the composition of the liquid at the $S/L$ interface. The model shows that alloy composition is critically important. The most effective solute elements have a high $Q$ value and a low $D$ value, which establishes that the undercooling needed to trigger nucleation events and facilitates their survival.[20] Moreover, the presence of potent nucleating substrates, through the term $\Delta T_n$, and their number density through the term $x_{sd}$ are influential as they provide heterogeneous nucleation sites in the CS zone. The Interdependence Model has been widely validated in a number of alloys such as Al, Mg, and Ti and for different solidification conditions such as ultrasonic treatment.[21–24] However, there are limited reports of incorporating the model with AM solidification conditions.[25,26] In addition, the interaction of multiple thermal cycles during AM makes the solidification process more complex than conventional solidification processing.

Significant grain refinement has been obtained in many cast alloy systems through the combined effects of solute and inoculants, using the current understanding of the underlying mechanisms which promote equiaxed grain morphologies.[21] This strategy has been extended to grain refinement of AM metals (*e.g.*, Al and Ti alloys), and recent progress will be reviewed in Section III. In addition to solute and inoculants, the process conditions of metal AM, such as the scanning parameters (*e.g.*, power, spot size, hatch spacing, scanning rate, *etc.*), can be manipulated to change the thermal gradient ($G$) and the solidification speed ($V$) in order to promote CET.[27,28] It is important to note that $V$ is sometimes denoted as $R$, as the growth rate of the $S/L$ interface, which is the microstructure response to the isotherm velocity or pull rate. While there is an important difference between the two,[29] in this paper, we are not differentiating the two as they are closely linked. Recent results show that CET can be achieved in some alloys by decreasing $G$ in the liquid region and increasing $V$ without adding alloying elements.[30,31] Additionally, adoption of physical processes (*e.g.*, ultrasonic treatment) has also shown remarkable grain refinement in metal AM and will be discussed in Section IV.

The purpose of this review is to understand the solidification conditions and the relationships between the solidification microstructure and grain refinement mechanisms for metal AM. The outstanding challenges to achieving uniform grain refinement throughout additively manufactured components are also discussed.

## II. SOLIDIFICATION CONDITIONS IN AM

As previously mentioned, AM is a generic name for a number of different layer-by-layer manufacturing processes which are all characterized by small melt pools, high cooling rates, and high thermal gradients in the melt.[32,33] This is confirmed both via experiments[34–46] as well as simulations[47–50] in a number of alloy systems. For instance, the cooling rates during powder bed fusion (PBF) processing of TiC/AlSi10Mg nanocomposites were determined to be in the order of $10^6$ K/s and thermal gradients were as high as $21.4 \times 10^6$ K/m.[51] Bermingham *et al.*[26] have reported cooling rates of $1\text{-}6 \times 10^2$ K/s with a thermal gradient during solidification of the order of $1\text{-}5 \times 10^5$ K/m for Ti-6Al-4V alloy processed by wire-arc AM (WAAM). Note that other AM processes might produce lower cooling rates and gradients, although they are still considered high compared to most casting processes.

It is a general observation in solidification processing that increasing the cooling rates decreases the grain size. This is true for AM processes also as summarized by Gorsse *et al.*[52] and Murr.[53] However, given the nature of AM processes with the simultaneous presence of high thermal gradients and cooling rates, understanding the mechanism of grain refinement in AM processes mandates grain size measurements to be made with quantifiable thermal gradients and cooling rates. This has been reported by Xu *et al.*[24] and Sun *et al.*[54] where higher cooling rates decreased the equiaxed grain size and higher thermal gradients had the opposite effect. Although the experiments were conducted with low cooling rates (of the order of 1 K/s), these results offer an important insight for understanding grain nucleation and its subsequent effect on the final grain size. Xu *et al.* explained their results on the basis of 'inhibited' and 'active' nucleation zones (discussed in detail later in this article) surrounding the growing grain, which are not different from the NFZ and CS-induced nucleation defined in the Interdependence Model.

Additionally, experimentally based research has shown that interesting microstructures are possible due to the solidification conditions present during the AM processes.[26,55] In the classical theory of growth kinetics, the $G/V$ ratio defines the morphology of the growing solid. A large $G/V$ value indicates the propensity for a planar solidification front to exist, while decreasing the $G/V$ value changes the growth mode from planar to dendritic and further changes the grain morphology from columnar to equiaxed. The relatively high positive thermal gradient present in the AM processes and the slow velocity of the $S/L$ interface in the early stages of solidification constrains the interface to grow with a columnar morphology in most cases.[56–58] It must be noted that AM processes may produce a fine microstructure, due to high $G \times V$ values, although with a columnar morphology. For example, Harrison *et al.*[55] reported columnar dendrites with an arm spacing of 1 $\mu$m in Hastelloy produced by laser powder bed fusion (L-PBF, often known as selective laser melting (SLM)). However, a challenge for AM processes is to produce a large portion of fine equiaxed grains. Recent results from experiments have shown encouraging results where a large area of fine equiaxed grains have been reported.[26,59] Numerical simulations have also shown similar possibilities where CET is favored when the thermal gradient is reduced.[57]

### A. *Manipulating the Solidification Conditions Using G-V Diagrams*

Conventional solidification theory suggests that equiaxed grains grow in a region where $G$ is negative.[60] Thus, CET necessarily requires that an undercooled region be present ahead of the growing columnar grains for equiaxed grains to nucleate and grow. While columnar growth necessitates the presence of a positive $G$ ahead of the $S/L$ interface, the role of $V$ in producing a solute diffusion field must also be recognized. Given that the interface growth rates control the morphology and the microstructure[61] of the solidifying system, a plot of $G$-$V$ offers a useful guide for engineering the final microstructure.

The CET models result in $G$-$V$ plots as originally developed by Hunt.[62] In turn, $G$-$V$ plots can be used to identify processing conditions to enhance or reduce CET (*e.g.*, Figure 1). The common feature in these plots is the boundary demarcating the equiaxed from the columnar grains and the $G$ and $V$ conditions required to achieve equiaxed grains. As such, the $G$-$V$ plots are useful for AM processes as well, but one of the limitations of the diagrams is that the inherent mechanisms of CET remains unknown. For instance, $G$-$V$ plots are often created for a given inoculant density.[62] It is now understood that the inoculant size determines the undercooling required for triggering a nucleation event[12,63] and that a large fraction of the inoculants remain unused. Nevertheless, $G$-$V$ diagrams are used to

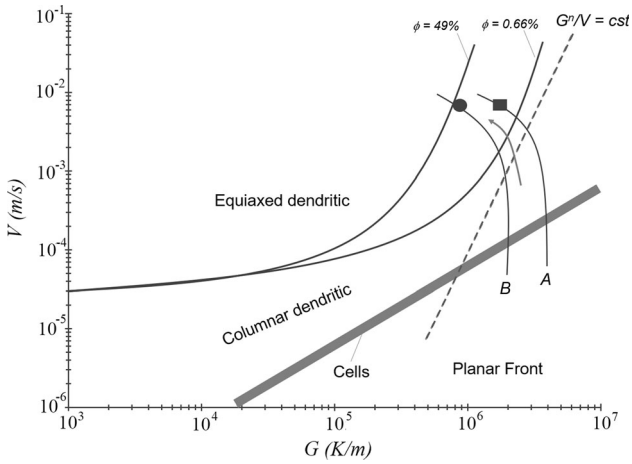


Fig. 1—Schematic of the $G$-$V$ plot adapted from Ref. [64]. The original plot was developed for a Ni-based superalloy based on numerical simulation of a laser melting process. $\varphi$ represents the extent of CET as proposed by Hunt[62]: $\varphi > 49$ pct, fully equiaxed grains *and* $\varphi < 0.66$ pct, fully columnar structure. 'A' and 'B' trace changes in the local thermal conditions during solidification as described in the text. 'Cst' in the figure is a constant which is a function of the alloy solidification range, alloy phase diagram, and nuclei density.

manipulate the processing conditions to engineer the desired microstructure and to study the CET in a number of alloys.[39,56,64,65]

*G-V* plots which have been developed for AM processes can be categorized under two groups—ones that use numerically calculated $V$ (in *G-V* plots),[58,65,66] and the ones which approximate the $S/L$ interface velocity using the scan speed of the energy source.[39] Given that the $S/L$ interface velocity controls the microstructure, it seems prudent to use $S/L$ interface velocity in such plots wherever possible,[64,66] especially since the actual $S/L$ interface growth rate may be spatially and temporally different in a given AM process.[57,58] Figure 1 shows the *G-V* plot using the numerically evaluated $S/L$ interface velocity for CMSX-4 Ni superalloy for the laser metal forming process.[64] Curves A and B in the plot show the change in $G$ and $V$ during solidification leading to the CET for two different conditions. The formation of equiaxed grains at low $G$ and high $V$ is clearly seen in the plot.

## B. *Modification of the Interdependence Model to AM*

One of the factors that has been often considered as an important reason for the prevalence of columnar grains is the very high $G$ experienced in AM processes compared to traditional manufacturing processes. A recent study by some of the authors has taken a more systematic approach to understanding the effect of solidification conditions in AM, by considering the analogous laser surface re-melting of a number of Al-Cu alloys grain refined without and with Al3Ti1B grain refiner additions.[67] While this study over-simplifies AM by considering only a single re-melted laser track, it provided insights into the difference between casting processes and AM (Figure 2).

While it is clear that having enough solute (*i.e.*, high enough $Q$-value) is critically important to achieve an equiaxed grain morphology in AM alloys,[26,68] this work[67] showed that in laser surface re-melted alloys varying the alloy composition has much weaker effect on the final grain size than that in cast alloys. Using the Interdependence Model to interpret the results, it was found that this was due to a much reduced length of the diffusion zone in front of the $S/L$ interface, often known as the NFZ due to the high growth velocities from the high cooling rates.

It was also shown that the number of grains that were nucleated on the added nucleant particles increased dramatically from less than 0.1 pct of the particles activating nucleation to 27 pct indicating a substantial number of lower potency nucleant particles that are effective in solidification conditions similar to AM. Particle size distributions typically show a larger fraction of particles of smaller size.[63] In a given AM process, the presence of deep thermal undercooling, although of short length, allows activation of smaller inoculants which require higher undercooling.[12,63] This large undercooling has the potential to enhance the CET, since a larger fraction of the available inoculants may be triggered. This suggests a much greater contribution of thermal undercooling to facilitate nucleation on less favorable grains.[29]

This means that while at lower $V$, the solute is a dominant player in providing the required undercooling[5]; it is the thermal undercooling that acts as a nucleation multiplier at high $V$ and high $G$. With shorter NFZ at high $V$ and steep $G$, the role of solute is restricted. This implies that alloys of two different compositions with the same inoculant chemistry and of similar size distribution would be expected to trigger an equally large number of equiaxed nucleation events.

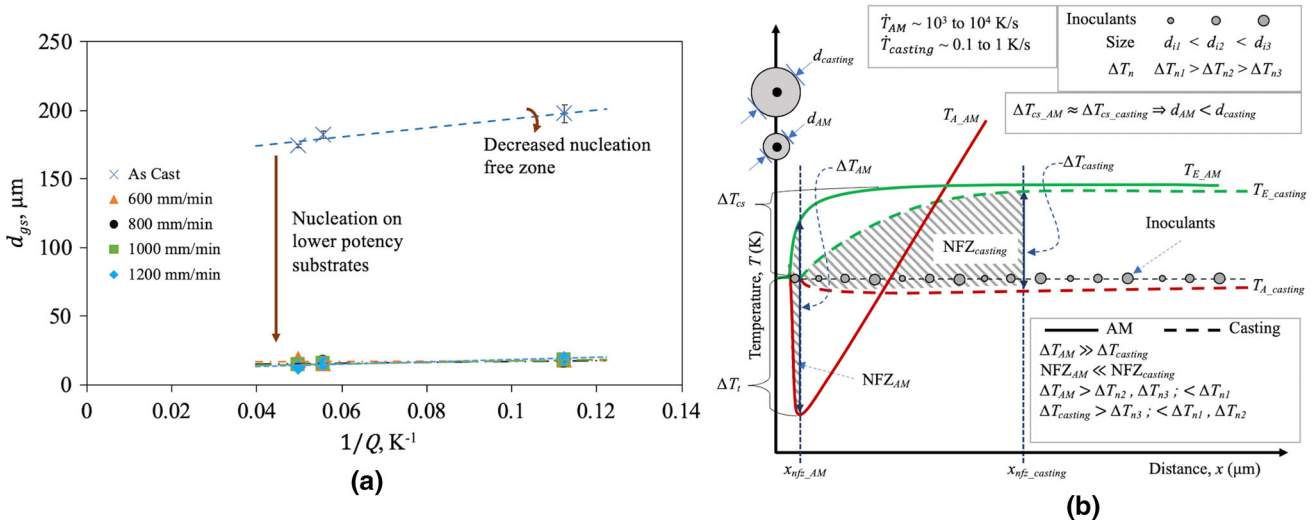


Fig. 2—(*a*) Al-Cu alloys grain refined by a 3 wt pct Al3Ti1B addition in the as-cast state and after laser surface re-melting (at 600, 800, 1000, and 1200 mm/min scan speed with 2 kW laser power), showing two predominant changes to the grain size. One is the reduction in the intercept which is typically understood as an increase in the number of particles available for nucleation. The other is the reduction in the gradient which is understood to be due to the reduction in the nucleation-free zone and in this case due to the reduction in the diffusion length of the solute. (*b*) Schematic showing the changes in the thermal fields in front of a grain for both, AM and casting processes. The NFZs for AM and casting are compared. Note schematic is not to scale. Reprinted from Ref. [67] with permission from Elsevier.

However, it appears that the situation is more complicated than this. One of the features in the work of Bermingham *et al.*[26] is the effect of recalescence on $G$, which in turn affects the solidification rate.[69,70] Recalescence and its effect on the solidification rate has been experimentally observed and reported recently *via in situ* synchrotron experiments.[71] It is to be noted that recalescence is likely in the case of a high number of equiaxed grain nucleation events and subsequent growth. Experimental results from Bermingham *et al.*[26] indicate that there exists a positive correlation between the presence of recalescence and the number of equiaxed grains formed. While the work reported a drop in the thermal gradient with consequent increase in equiaxed nucleation events, further experimental validation would be useful. In addition, modeling efforts to further understand the role of recalescence would be valuable.

To model AM processes effectively, solidification models must also incorporate non-equilibrium solidification conditions, where high interfacial growth rates may result in solute trapping, thereby modifying the partition coefficient and the alloy liquidus slope. Extremely high cooling rates ($> 100$ K/s) are expected in AM processes where the non-equilibrium effects may become active.

In summary, to generate a fine equiaxed grain structure during AM processes, the solidification conditions present in AM processes require manipulation of a combination of thermal gradient, cooling rate, alloy composition, and grain refiners (chemistry, inoculant number density, and size distribution). The following sections discuss the role of alloy chemistry and the use of external fields to modify these factors to achieve the goal of obtaining an equiaxed grain structure.

## III. GRAIN REFINEMENT BY ALLOYING ADDITIONS

### A. *Titanium Alloys*

The Ti system is perhaps the most suited for and, therefore, widely studied alloy system for AM on the basis of its high material cost and the difficulties associated with conventional processing (such as machining and casting). Unlike other alloy systems where there is usually a clear distinction between foundry and wrought alloys, all commercial Ti alloys developed for casting have chemical compositions based on wrought alloys, of which Ti-6Al-4V is used in around 90 pct of casting applications.[72] Consequently, Ti-6Al-4V is also the pre-eminent alloy for AM. Despite containing 10 wt pct solute, Ti-6Al-4V behaves much like a pure metal during solidification with a narrow freezing range and, thus, has good properties for solidification processing (*e.g.,* good fluidity, low susceptibility to hot tearing and other solidification defects *etc.*). This is because Al and V solute both have high solid solubility (low $Q$-value) and do not readily partition into the liquid*.[73] Consequently, cast and additively manufactured Ti-6Al-4V both have a coarse prior $\beta$-Ti grain size similar to pure Ti.

The suitability of Ti-6Al-4V for melt processing, combined with the fact that this alloy derives most of its desirable structural properties from solid solution strengthening and the morphology of the $\alpha + \beta$ phases that form, has stifled innovation in new alloy development for solidification processing. Nevertheless, there have been efforts to develop grain refiners for this and other Ti alloys where fine equiaxed grain sizes are desired. To the authors' best knowledge, the earliest such report was in 1970 when Samsonov *et al.*[74] added various elements to pure Ti sponge. The results revealed that some elements including La, Y, Ni, and Co are considerably more effective grain refiners than others. Little was known at the time about the mechanisms for this refinement, but subsequent research has provided substantial insights and it is likely that both solute and nucleant particle refinement effects are at play. These same principles are transferable to AM, and here, we briefly summarize the advances made in chemical grain refinement of Ti alloys produced by AM.

Grain refinement of AM Ti alloys has so far mainly focused on alloy design incorporating solutes that generate CS (*i.e.*, high $Q$-value solutes). Table I shows a shortlist of calculated and experimentally determined growth restriction factors for various solutes in Ti (for the full list interested readers are referred elsewhere[73,75]). It is worth noting that this is a calculated list based on binary phase diagram information and does not consider ternary reactions.

Boron is among the most powerful growth restricting solutes in the Ti system and has been investigated as a grain refiner during AM. The high potency of boron means that small additions (*i.e.*, $< 0.5$-1 wt pct) have strong refinement effects, which makes mixing and alloying of powders for AM achievable. Boron not only refines the $\beta$-Ti grain size, but also refines the $\alpha$-lath size and produces more equiaxed $\alpha$-grains. Consequently, boron has been used to refine the grain size in Ti alloys produced by WAAM[81,82] and laser-directed energy deposition (L-DED, often known as laser metal deposition (LMD)).[83–87] Other growth restricting solutes including carbon,[80] tungsten,[79] silicon,[88] copper,[68] nickel[89], and chromium[26] have also proven to be effective in $\beta$-Ti grain refinement during AM. Broadly speaking, the effectiveness of solutes in refining $\beta$-Ti grains during AM is in line with their growth restriction factor. Figure 3 shows some examples of refinement of Ti alloys produced by AM through alloy design with high $Q$-solutes.

An ongoing challenge in forming equiaxed grains during AM of Ti alloys is the current lack of available potent nucleant particles. It is often reported that columnar grain width decreases when high $Q$-solutes are added during AM, but the CET fails to occur. To date, there has been little insight into what foreign particles can catalyze heterogenous nucleation of $\beta$-Ti grains at small $\Delta T_{n.}$ It is known that Ti alloys naturally

*During the solid transformation from $\beta \rightarrow \beta + \alpha$, segregation of Al and V does occur, however, in the liquid segregation is limited.

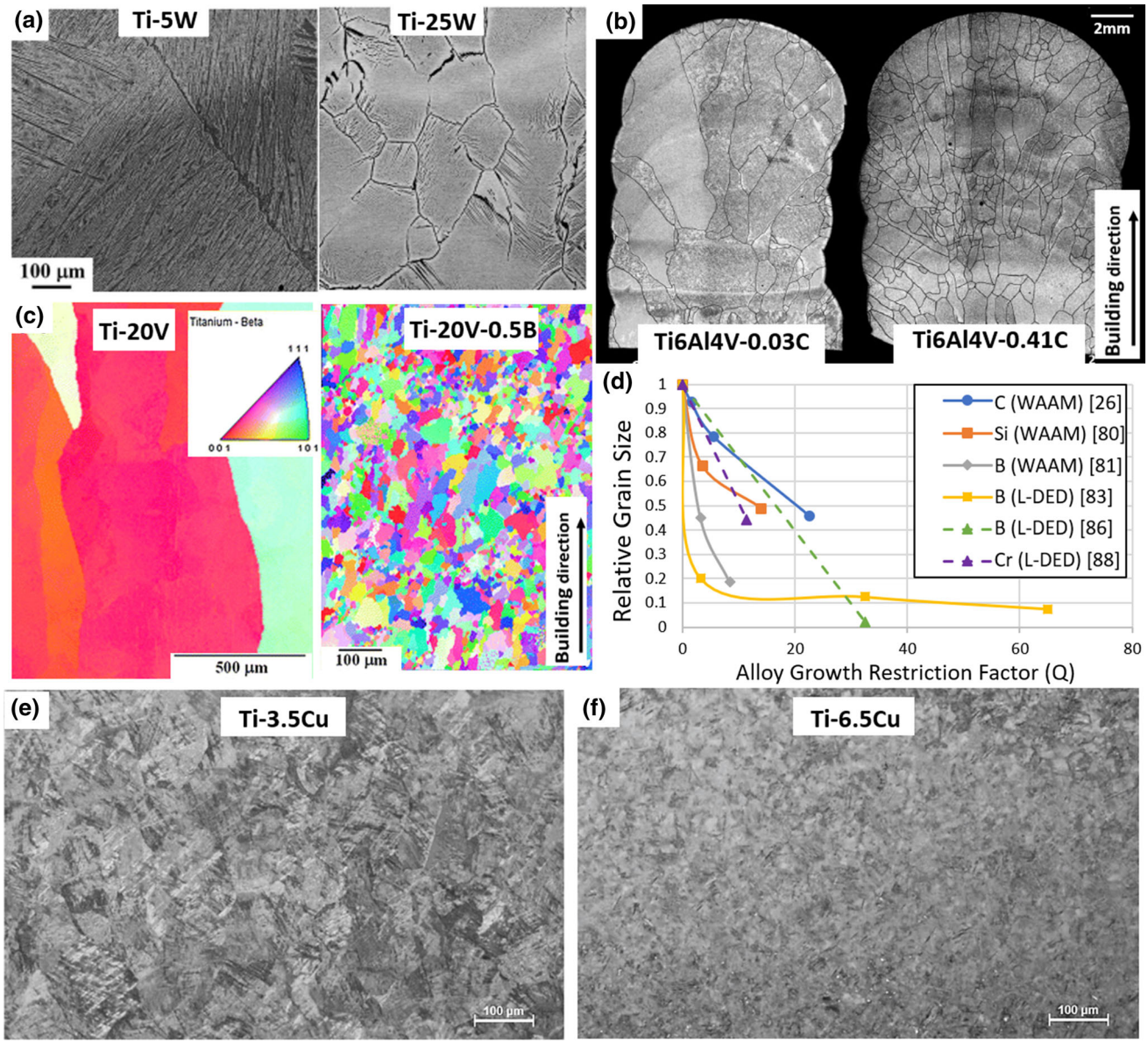


Fig. 3—(*a*) Refinement of $\beta$-Ti grains during L-DED with tungsten addition, reprinted from Ref. [79]; (*b*) Refinement of $\beta$-Ti grains during WAAM with carbon addition, reprinted from Ref. [80]; (*c*) Refinement of $\beta$-Ti grains during L-DED with boron addition, adapted from Ref. [83]; (*d*) The effect of growth restricting solute on the grain size of Ti alloy produced by AM (increasing $Q$ causes significant reduction in grain size).[26,80,81,83,86,88] Relative grain size is expressed as a fraction of 1 which represents the base unrefined alloy, such as Ti-6Al-4V. (*e*, *f*) Polarized optical microscopy images showing the equiaxed grains of as-printed Ti-3.5Cu and Ti-6.5Cu alloys produced by L-DED, reprinted from Ref. [68] with authorship permission.

contain a population of 'native' particles that are capable of seeding equiaxed grains under appropriate conditions (*i.e.,* in supercooled melts),[73,90], but the identification of these particles remains unknown. Tedman-Jones and co-workers investigated if these particles originate during Ti sponge production, in particular the metal salts used during the Kroll or similar processes, and found that Na and Cl impurity compounds enhanced the nucleation rate of $\beta$-Ti grains.[91] Although the exact particle responsible for nucleating $\beta$-Ti grains was not identified, it lays the groundwork for future research to successfully isolate and then intentionally alloy these particles with Ti for the purposes of grain size and morphology control during AM (*i.e.,* reducing the $x_{sd}$ term of the Interdependence Model).

Other particles that have been used to nucleate $\beta$-Ti grains include W,[92] Mo,[92] Nb,[92] TiN,[93] $La_2O_3$[26], and even unmelted Ti particles.[90,94,95] These can largely be grouped as either being transient or stable, where transient particles such as unmelted Ti, Mo, W, or Nb powders can temporarily survive in the melt pool long enough for solidification to occur, but are subject to dissolution over extended periods in contact with the melt pool, as shown in Figure 4. Such particles have

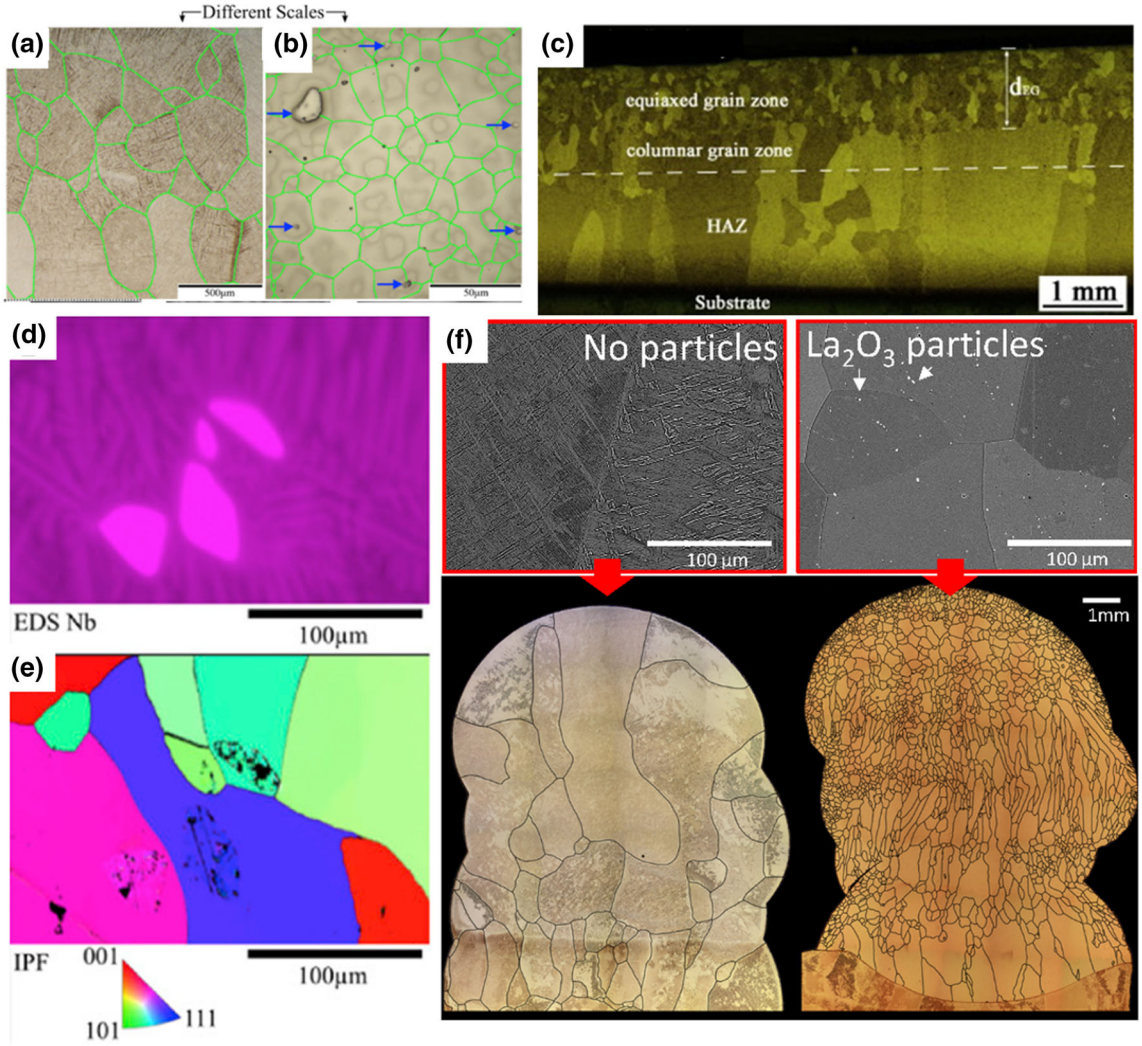


Fig. 4—Nucleant particles can substantially refine the grain size of titanium alloys produced by AM. (*a*, *b*) The grain size in WAAM is reduced by an order of magnitude with the addition of *W* particles (note images are at different magnifications)[92]; (*c*) Fine equiaxed grains nucleate on unmelted powder particles during L-DED[94]; (*d*, *e*) Nb particles nucleate $\beta$-Ti grains during WAAM[92]; (*f*) $La_2O_3$ particles refine the grain size of Ti alloys during WAAM.[26] All figures are reprinted with permission from Elsevier.

been exploited for grain size control in WAAM and L-DED processes, but are sensitive to the processing conditions that determine whether or not the particles melt or dissolve, in which case they are unavailable to nucleate grains.

Peritectic forming elements N, O, and C have been used to refine the grain size in cast Ti alloys as far back as the 1980s.[96,97] The mechanism for peritectic grain refinement involves firstly the nucleation of pro-peritectic particles (*e.g.*, TiN) that then nucleate the $\beta$-Ti phase. This principle was latter used by Qiu *et al.*,[93] who achieved refined equiaxed grains through the addition of ZrN to a $\beta$-Ti alloy which later decomposed in the melt to form TiN that nucleated the $\beta$-Ti phase. Although the solute components of these additions may also provide grain refinement through the growth restriction mechanism (refer to Table I), similar studies in other alloy systems have shown that the predominant refinement can be attributed to nucleation on the pro-peritectic phase.[98] The downside to this method of grain refinement is that no peritectic reactions occur in Ti at trace compositions, and hence, large mass fractions of usually embrittling alloy elements are required (*e.g.*, as in the case of O, N and C). The peritectic reaction between Ti and La has been exploited to produce equiaxed $\alpha$-Ti grains during L-PBF of a Ti-2La alloy.[99]

Rare earth elements and their oxides have also been reported as promising grain refiners for $\beta$-Ti for a number of decades and have recently been applied to AM. $La_2O_3$ particles were used by Bermingham *et al.* to promote the CET and achieve a grain size reduction of 85 pct compared to Ti-6Al-4V.[26] $Ce_2O_3$ and $Y_2O_3$ particles are also reported to refine the grain size of laser-re-melted Ti welds.[100] A benefit of rare earth oxides is that they are among the few particles that may be stable in liquid Ti, an essential requirement for any

**Table I. List of Growth Restriction Factors ($Q$ Values) for Solutes in the Ti System**

| Element | $m$ | $k$ | Concentration (Wt Pct) | $Q$* | References |
|---|---|---|---|---|---|
| Al | − 1.7 | → 1 | up to 20 pct | → 0 | [76] |
| V | − 2 | → 1 | up to 12 pct | → 0 | [77] |
| Sn | − 0.8 | 0.92 | up to 35 pct | 0.06 | [77,78] |
| Nb | 3.4 | 1.08 | up to 25 pct | 0.27 | [77,78] |
| Zr | − 2.3 | 0.86 | up to 55 pct | 0.34 | [77,78] |
| Mo | 6.5 | 1.08 | up to 30 pct | 0.52 | [77,78] |
| Cr | − 8.1 | 0.76 | up to 15 pct | 1.5 | [75] |
| Fe | − 18 | 0.82 | up to 5 pct | 3.2 | [75] |
| La | − 5.7 | 0.43 | up to 21 pct | 3.3 | [77] |
| Nd | − 4.6 | 0.27 | up to 12 pct | 3.4 | [77] |
| Ce | − 6.1 | 0.19 | up to 4 pct | 4.9 | [77] |
| Er | − 6.6 | 0.15 | up to 3 pct | 5.6 | [77] |
| Y | − 6.7 | 0.08 | up to 45 pct | 6.2 | [77] |
| Cu | − 10.6 | 0.39 | up to 18 pct | 6.5 | [75] |
| Pd | − 23.9 | 0.7 | up to 5 pct | 7.2 | [77] |
| Mn | − 15.3 | 0.5 | up to 4 pct | 7.7 | [77] |
| Ta | 16.5 | 1.48 | up to 30 pct | 8.0 | [77] |
| O | 27.6 | 1.37 | up to 1.5 pct | 10.8 | [75] |
| Sc | − 18.8 | 0.39 | up to 14 pct | 11.4 | [77] |
| Ni | − 23.8 | 0.40 | up to 5 pct | 14.3 | [75] |
| Co | − 24.1 | 0.20 | up to 5.5 pct | 19.2 | [77] |
| Si | − 32.5 | 0.35 | up to 4 pct | 21.7 | [75] |
| W | 15.1 | 2.50 | up to 4 pct | 22.7 | [79] |
| C | − 55 | → 0 | up to 0.5 pct | 55 | [80] |
| B | − 65 | → 0 | up to 1.6 pct | 65 | [77] |
| Be | − 86 | 0.19 | up to 8 pct | 72 | [77] |

*The $Q$-values are shown for 1 wt pct solute, but will vary on actual alloy composition.

nucleating particle. La, Y and other rare earths have been reported to refine the grain size in welds, which have comparable solidification conditions to some AM processes.[100–103] Although some of these rare earth elements are also growth restricting in the Ti system (see Table I), it is likely that they scavenge oxygen to form oxide particles within the molten Ti pool, which may be responsible for nucleating $\beta$-Ti.

The identification of new potent nucleant particles is essential for controlling the grain size and morphology during AM of Ti alloys. Several studies have shown that it is possible to produce equiaxed grains during AM; however, an ongoing challenge is to ensure completely homogenous microstructures. Often mixed columnar and equiaxed structures are reported. Complete elimination of columnar grains during AM (preventing epitaxial growth) will require highly potent nucleant particles to be discovered. Of course, the addition of grain refiners must not impair other alloy properties which is something that will require ongoing work.

## B. *Aluminum Alloys*

Research into AM of Al alloys has been somewhat limited compared to other alloy systems, despite their use in numerous applications in the automotive, aerospace, and consumer goods industries.[104–107] For example, a recent review of metal AM revealed that only 15.6 pct of research articles are published since year 2007 that are focussed on Al, compared to 34.8 pct and 36.3 pct for steels and Ti alloys, respectively.[108] Furthermore, a number of factors complicate AM of Al alloys, including, but not limited to oxides on the surface of the powders, poor flowability of the powder, low absorptivity of Al alloys to wavelengths characteristic of some laser sources, and high material thermal conductivity.[109] The low absorptivity and high thermal conductivity necessitate the use of high energy inputs in order to melt the powder, which can further complicate the process by leading to the preferential vaporization of high vapor pressure alloying elements such as Zn and Mg.[110–115]

The current literature on AM of Al alloys can broadly be grouped into two groups of alloys. The first group is the high Si content Al-Si casting alloys, which offer good fluidity and low levels of solidification shrinkage.[115,116] Of these alloys, Al10SiMg has been the most widely studied and has been shown to have similar or higher strength properties compared to cast samples of the same alloy.[117,118] However, it is known that Si contents above 2 to 3 wt pct can increase the grain size in traditional castings[119] despite their high $Q$-value (-Table II). So AM of the Al-Si alloys often results in a columnar grain structure oriented parallel to the build direction.[117,120] Consequently, as-deposited Al-Si alloys often display anisotropy in their mechanical properties.[117] The second group of alloys are the precipitation-strengthened Al alloys, such as the 2xxx (Al-Cu-Mg), 6xxx (Al-Mg-Si), and 7xxx (Al-Zn-Cu-Mg) alloys, typically used as wrought alloys. However, these alloys tend to have lower Q-values (Table II), necessitating the use of grain-refining master alloys and also

Table II. List of Some AM Al Alloys with the $Q$ Values, Based on the Composition Given in References

| Alloy, Composition in Wt Pct | $Q$ (Approx.), K | References |
|---|---|---|
| AlSi10Mg, (Al-10Si-0.32Mg-0.03Cu) | 60 | [124] |
| AlSi10Mg/$TiB_2$, (Al-9.81Si-0.32Mg-0.02Cu-0.01Mn-3.84Ti-1.8B) | 91.9 | [124] |
| 6061, (Al-0.65Si-0.86Mg-0.1Mn-0.55Fe-0.3Cu-0.03Zn-0.15Cr-0.02Ti) | 13.8 | [125] |
| 6061/TiBor®, (Al-0.65Si-0.8Mg-0.1Mn-0.61Fe-0.28Cu-0.03Zn-0.14Cr-0.34Ti-0.06B) | 42.3 | [125] |
| 7075, (Al-5.4Zn-2.25Mg-1.54Cu-0.19Cr-0.17Fe-0.13Si-0.02Mn) | 13 | [106] |
| Al-Mn-Mg-Sc, (Al-4.52Mn-1.32Mg-0.79Sc-0.74Zr-0.05Si-0.07Fe) | 5.7 | [132] |

The $m(k-1)$ values for the alloying elements were obtained from previous work Easton 2005.[129–131] Sc has little or no growth restricting ability in Al-based alloys, so its contribution was assumed to be negligible. The contribution of the elements to $Q$ was limited to their solubility in liquid Al just prior to solidification.

they tend to have a large solidification temperature range at the final stages of solidification making them more susceptible to hot tearing (cracking) during solidification.[106,115,116,121,122] Moreover, AM of the precipitation-hardened alloy series often leads to variable compositions through the height of the deposited material, due to preferential evaporation of Zn and Mg. Nevertheless, these alloy series are of interest for AM, as the strength of the deposited material can be significantly increased using a simple aging heat treatment. A number of approaches have been undertaken to improve the processability of Al alloys in AM and to control the microstructure and resultant properties of the deposited material. In particular, methods to achieve grain refinement by modifying the alloy composition have been adopted from the well-established casting literature.

The most common grain refinement method in casting is the addition of an Al-Ti-B master alloy to the melt, in which the Ti content is usually above the $TiB_2$ stoichiometric ratio of 2.2:1 (wt pct). This provides $TiB_2$ inoculant particles, which are believed to contain an intermediate $Al_3Ti$ layer to facilitate nucleation, as well as Ti solute, which has an extremely high relative $Q$ value in Al alloys.[98,123] Given the success of Al-Ti-B grain refiners in achieving grain refinement in castings, they have been added to Al alloys in AM processes and substantial grain refinement has been reported. Effective grain refinement of Al10SiMg produced by L-PBF was noted by decorating the powder particle surface with nanoscale $TiB_2$ particles (5.6 wt pct) as seen in Figures 5(a) and (b).[124] Carluccio *et al.*[125] added 0.33 wt pct Al5TiB grain refiner to Al-7Si and 6061 alloys, which were then subjected to laser re-melting. Significant grain refinement was noted for all scan speeds studied; at the lowest scan speed, the average grain size decreased from around 33 $\mu$m to 5 $\mu$m for 6061 and from 30 $\mu$m to under 10 $\mu$m for Al-7Si. Wang *et al.*[126] used L-PBF for *in situ* fabrication of a $TiB_2$/Al-3.5Cu-1.5Mg-Si composite by blending 5 vol. pct $TiB_2$ powder particles with the base alloy, and an order of magnitude decrease in the grain size was reported with the $TiB_2$ additions, from 23 $\mu$m to 2.5 $\mu$m. Wen *et al.*[127] added 3 wt pct $TiB_2$ to 2024 in a laser solid forming process and achieved equiaxed microstructure having a grain size range of 20-35 $\mu$m with increased mechanical performance of components compared to long columnar grains with width ranging from 60 $\mu$m to 1.6 mm in 2024 without the grain refiner. Most recently, $LaB_6$ has also been shown to be an effective nucleant particle during L-PBF of Al10SiMg, as shown in Figures 5(c) and (d).[128]

The addition of Zr has also proven to be effective in refining the as-deposited microstructure of Al alloys in AM. During solidification, $Al_3Zr$ particles first form in the melt. As the melt pool continues to cool, the $Al_3Zr$ particles provide heterogeneous nucleation sites for the primary $\alpha$-Al phase[133] and what is sometimes called the peritectic reaction and transformation occurs.[98] The addition of Zr powder has been shown to produce an equiaxed microstructure for L-PBF of Al-Cu-Mg alloys.[121,122] The as-deposited microstructure was observed to transform from one consisting of equiaxed grains at the melt pool boundary and columnar grains growing toward the center of the melt pool to one consisting of a homogeneous distribution of equiaxed grains 1 to 2 $\mu$m in size.[121] Furthermore, it was noted by Zhang *et al.*[122] that the amount of equiaxed grains depended on the scan speed, with a fully equiaxed structure observed for a scan speed of 5 m/min, but a heterogeneous microstructure of equiaxed and columnar grains when the scan speed was 15 m/min. Martin *et al.*[106] also used Zr additions to transform the L-PBF as-deposited microstructure of 7075 and 6061 alloys from columnar to equiaxed, by decorating the powder particle surfaces with $ZrH_2$ nanoparticles (Figures 5(e) and (f)). It is worth noting at this point that in the cases where Zr additions altered the microstructure from columnar to equiaxed grains, hot tearing was also effectively eliminated. Grain refinement has been achieved with pre-alloyed Al-Mg-Zr powder, in which the microstructure is again characterized by fine equiaxed grains at the melt pool boundary and coarser columnar grains growing into the melt pool.[134,135] The $Al_3Zr$ particles were observed at the center of the equiaxed grains, but were absent in the columnar grain region. It should also be noted that the extent of grain refinement depends on the amount of Zr addition; Yang *et al.*[136] noted epitaxial growth of columnar grains over ~ 20 layers in an Al-Mg-Zr alloy with only 0.21 wt pct Zr.

Grain refinement has also been achieved through the addition of Sc, particularly for the Al-Mg alloys. Similar to Zr, $Al_3Sc$ particles in the melt pool provide heterogeneous nucleation sites for the primary Al. An additional benefit of using Sc additions in AM processes is

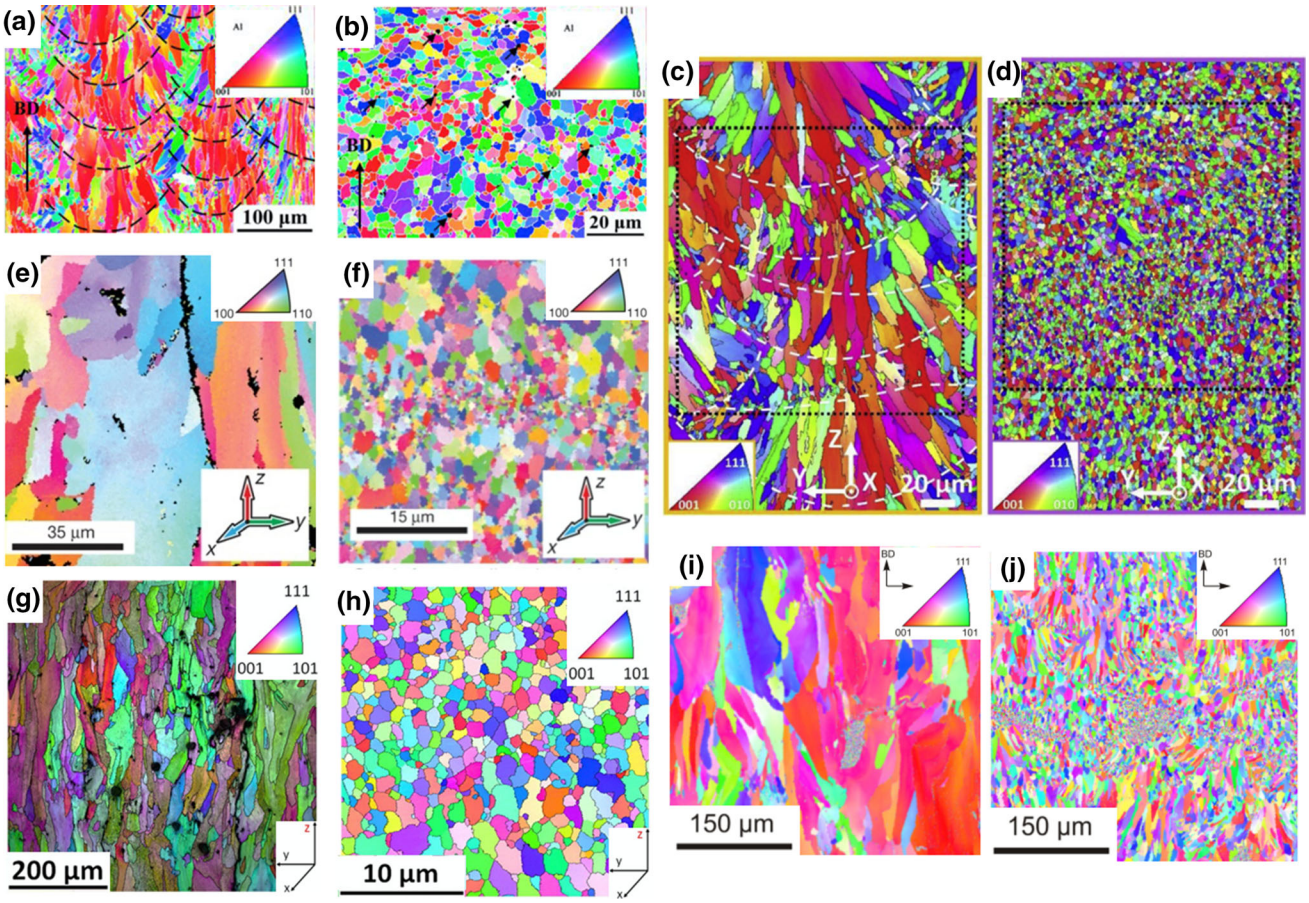


Fig. 5—Grain refinement of Al alloys by solute and particle addition in L-PBF. Electron backscatter diffraction (EBSD) maps of (*a*) Al10SiMg, (*b*) $TiB_2$/Al10SiMg,[124] (*c*) Al10SiMg, (*d*) $LaB_6$/Al10SiMg,[128] (*e*) Al7075, (*f*) Zr/Al7075,[106] (*g*) Al-Mg-Zr, (*h*) Sc/Al-Mg-Zr,[136] (*i*) Al7075, and (*j*) Si/Al7075.[115] Note the difference in scale bars between the examples. (*e*, *f*) are reprinted with permission from Springer Nature and the others are reprinted with permissions from Elsevier.

that higher levels of Sc solid solubility are possible due to the rapid solidification rates, which leads to the precipitation of coherent nanoscale $Al_3Sc$ strengthening particles upon subsequent heat treatment.[137] The addition of Sc leads to a microstructure characterized by fine equiaxed grains at the melt pool boundaries and columnar grains growing toward the center of the melt pool.[138] However, the proportion of the microstructure characterized by equiaxed grains has also been found to depend on the processing conditions. For example, Yang *et al.*[136] found that the volume fraction of equiaxed grains increased when the build platform was heated to 200 °C compared to 35 °C, and the fraction of equiaxed grains further increased to 100 pct as the volumetric energy density increased. Figure 5(g) displays the as-deposited microstructure without Sc, while Figure 5(h) reveals a homogeneous equiaxed morphology when a Sc-modified alloy was deposited on a 200 °C build plate. A similar effect of base plate heating was observed by Shi *et al.*,[139] but a fully equiaxed microstructure was not observed. Zhou *et al.*[140] found a similar grain refinement effect in Al-6Zn-2Mg with 1 wt pct (Sc + Zr) additions, where equiaxed grains exist at the re-melt boundary and columnar grains extend toward the center of the melt pool. It was proposed that the equiaxed grains exist only at the re-melt boundary where the peak temperature remains below 800 °C and the $Al_3Sc$ particles are stable. When the temperature exceeds 800 °C in the melt pool and $Al_3Sc$ particles are not stable, there is columnar growth. However, a consideration of Table II also shows that the current Sc-containing alloys tend to have a low *Q*-value indicating that while they have potent nuclei the alloys do not generate a lot of CS, which consequently means that columnar growth is more likely especially at higher thermal gradients. Nevertheless, the grain refinement observed at the re-melt boundary was found to prevent hot tears in the deposited material.

In a similar manner to using an Al-Si filler wire to weld crack-susceptible 7xxx alloys,[141] Montero-Sistiaga *et al.*[115] blended up to 4 wt pct Si powder with pre-alloyed 7075 powder to eliminate cracking in L-PBF. While hot tearing was completely eliminated with the addition of 3 wt pct Si, a corresponding change in the microstructure was also noted. Coarse columnar grains were aligned along the build direction in the baseline 7075 alloy (Figure 5(i)). However, the columnar grains became more refined with Si additions, and

clusters of equiaxed grains were eventually observed to disrupt the columnar grains (Figure 5(j)).

At the present time, opportunities still abound to translate grain refinement knowledge from casting to AM. There is a possibility of further investigating the role of peritectic elements and the role of eutectic growth restricting elements as well.

### C. *Other Alloy Systems*

There are a number of other alloy systems that have been studied in AM, particularly Fe-based, Ni-based, and Co-based alloys. Grains of columnar morphology are also typical in these alloy systems (Figure 6).

These alloy systems have not been extensively studied for grain refinement during AM, but there have been a few successful attempts in introducing inoculants to

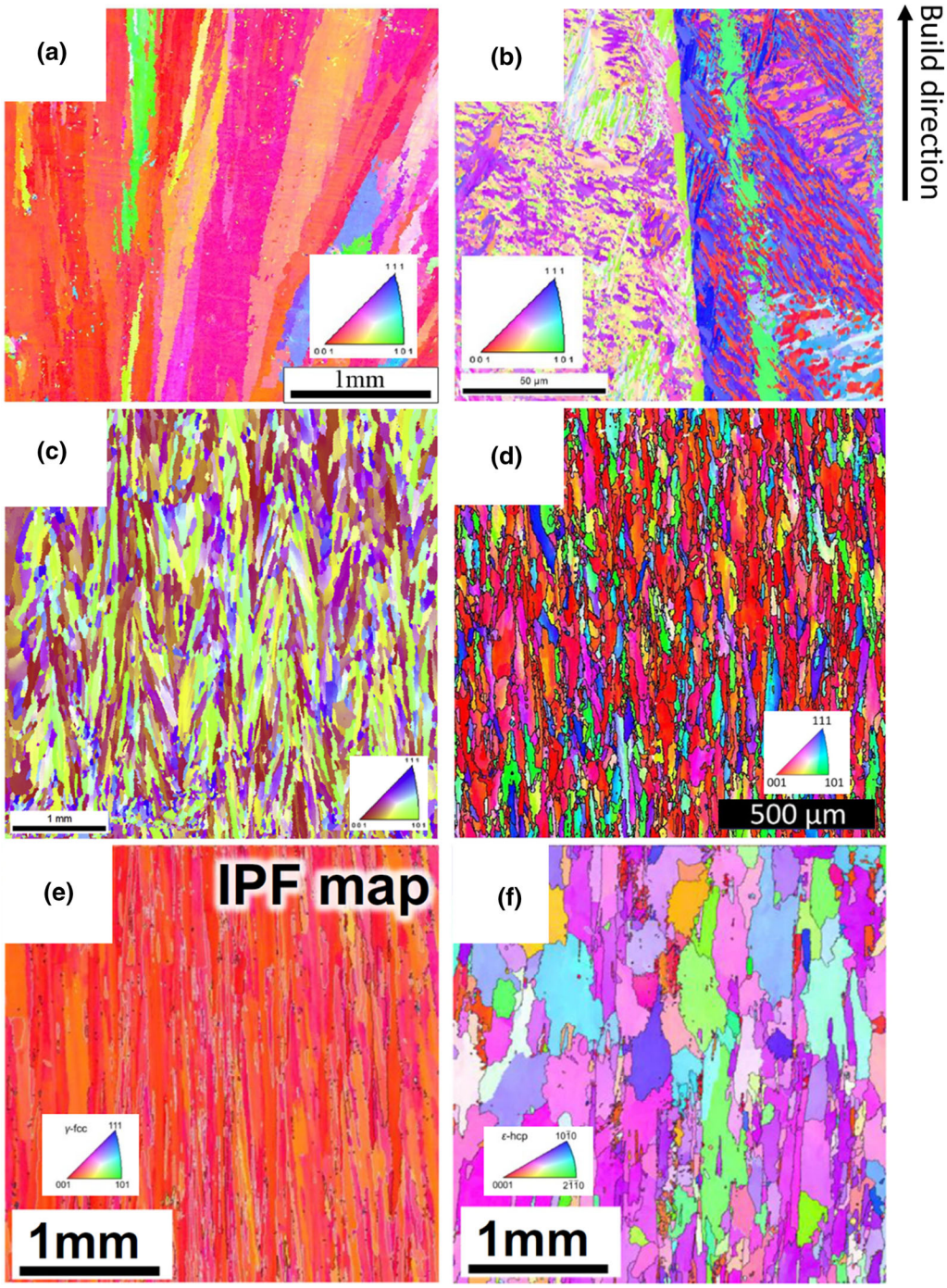


Fig. 6—Examples of columnar grain structures in (*a*) 316L steel by WAAM,[142] (*b*) AerMet100 steel by L-DED,[143] (*c*) IN718 alloy by electron beam powder bed fusion (EB-PBF),[58] (*d*) IN625 by L-PBF,[144] (*e*, *f*) Co-Cr-Mo alloy by EB-PBF at different heights of as-built rod: (e) bottom and (f) top of part.[145] All figures are reprinted with permissions from Elsevier.

stainless steels and Ni-based superalloys.[146–149] For example, AlMangour *et al.*[146,147] added 15 pct vol of TiC nanocrystalline into H13 steel fabricated using L-PBF with different scanning strategies. The results showed that elongated columnar grains are dominated along the building direction, but a "cross-hatching" scanning strategy (*i.e.*, the scanning direction is altered 90 deg between consecutive layers) was shown to reduce the grain texture and thus minimize the anisotropic properties. Li *et al.*[148] produced 316L stainless steel with the addition of 3 wt pct submicron-sized $V_8C_7$ particles by L-PBF and found that the austenite phase grains can been refined as *in situ* formed $VC_x$ nanocrystalline particles act as nucleation sites and have the further effect of pinning grain boundaries. For Ni-based superalloys, Ho *et al.*[149] investigated the microstructure evolution of eutectic WC-$W_2C$ inoculants in IN718 produced by L-PBF. The results suggested that eutectic WC-$W_2C$ inoculants can provide heterogeneous nucleation sites for grain formation and thus small grains nucleate along the surface of the inoculants. Overall, introducing inoculants to the above alloys can refine grains to a certain extent and more investigation is needed. However, it seems that other approaches are needed to grain refine such alloys. One approach to promote grain refinement is to use mechanical techniques or process control, which can be applied across all alloy systems.

## IV. GRAIN REFINEMENT BY MECHANICAL APPROACHES OR PROCESS VARIATIONS

Although grain-refining master alloys are widely used for solidification control, inoculant particles tend to accumulate and may become entrapped as inclusion defects in metallic components.[150] The use of external fields during solidification is an emerging alternative approach for microstructure control, which achieves grain refinement without the addition of chemical refiners. The literature on external fields for solidification processing largely deals with application to conventional casting processes.[151–159] In the casting industry, the widespread adoption of external fields has been hindered by difficulties in treating large volumes of liquid metal. However, an entire additively manufactured part can in principle be effectively treated since the melt pool volume is quite small (generally ~ 0.1-1.0 mm in width).

Only a few studies have applied external fields during AM. In contrast, external fields have been used during welding by many techniques including high-intensity ultrasound,[160–164] energy source oscillation[165–169] and energy source pulsing.[166,170–175] In each case, the applied external field vigorously agitates the solid front to enhance nucleation or substantially increase the number of crystallites during solidification. In this regard, the use of external fields stands out as a significant opportunity for microstructure control during AM without changing alloy chemistry.

The application of high-intensity ultrasound (vibrations exceeding the range of human hearing, *i.e.*, $> 20$ kHz) during solidification of metals and alloys introduces an alternating sound pressure to the melt, which can initiate acoustic cavitation (the formation, growth and implosive collapse of bubbles). Cavitation can trigger grain refinement by dendrite fragmentation and/or enhanced nucleation. Both mechanisms have been critically reviewed previously[176,177] and will not be further discussed herein. Coupling ultrasonic vibration to the melt pool during AM is a major challenge, although inspiration can be drawn from welding studies.

Vibrating the workpiece (either longitudinal or transverse to the travel direction of the heat source) at a frequency of 19 to 20 kHz can promote grain refinement in small melt pools of welds.[160–162,164] From the perspective of AM, grain refinement by this technique was demonstrated by Todaro *et al.*[178] (Figure 7). By embedding a vibrating ultrasound sonotrode (20 kHz frequency, 30 $\mu$m amplitude) in the build plate of a L-DED system, coarse columnar grains were effectively replaced by fine equiaxed grains with reduced crystallographic texture in both Ti-based alloy Ti-6Al-4V (Figures 7(a) and (b)) and Ni-based alloy Inconel 625 (Figures 7(c) and (d)).[178] Similar results were obtained in independent experiments using Al-based alloy Al-10Si fabricated by L-DED with ultrasound.[179] It is noted that this approach does not allow the workpiece to be clamped down as required to avoid distortion of metallic build plates, which could be an important practical consideration when additively manufacturing large parts.

Alternatively, ultrasonic grain refinement may occur during AM by directly inserting an ultrasound sonotrode into the melt pool. This method permits the AM build plate to be clamped. This approach was first demonstrated by Yuan *et al.*[163] during arc welding of Mg-based alloys AZ31 and AZ91 using a 0.5 mm diameter tungsten ultrasound sonotrode vibrated with a frequency of 20 kHz. Figure 8 shows an example of an ultrasonically treated Mg-based alloy AZ31 weld (Figure 8(a)), where full transition from columnar grains (Figure 8(b)) to equiaxed grains (Figure 8(c)) occurred by the application of ultrasound. The notable findings of Yuan *et al.*[163] include the following: (1) increasing the ultrasonic amplitude from 14 $\mu$m to 28 $\mu$m reduced the grain size, (2) the higher solute-containing alloy (AZ91) welds exhibited finer grains both with and without ultrasound, and (3) increasing the growth velocity $v$ decreased the grain size both with and without ultrasound. Using the Interdependence Model (Eq. [2]), increasing the ultrasonic amplitude activates a larger proportion of nucleant particles[180] (possibly by reducing $x_{sd}$[181]), while increasing both the growth velocity $v$ and growth restriction factor $Q$ reduces the size of the NFZ $x_{nfz}$. These effects contribute to a finer grain size $d_{gs}$ according to the Interdependence Model.

Ultrasonic grain refinement should be easily implementable in L-DED and WAAM processes. The application of the technique to PBF processes is challenging since vibration is expected to disrupt the layer of powder after recoating. Regardless, the advantage of controlling the grain structure of additively manufactured parts without modifying alloy chemistry[178] may trigger

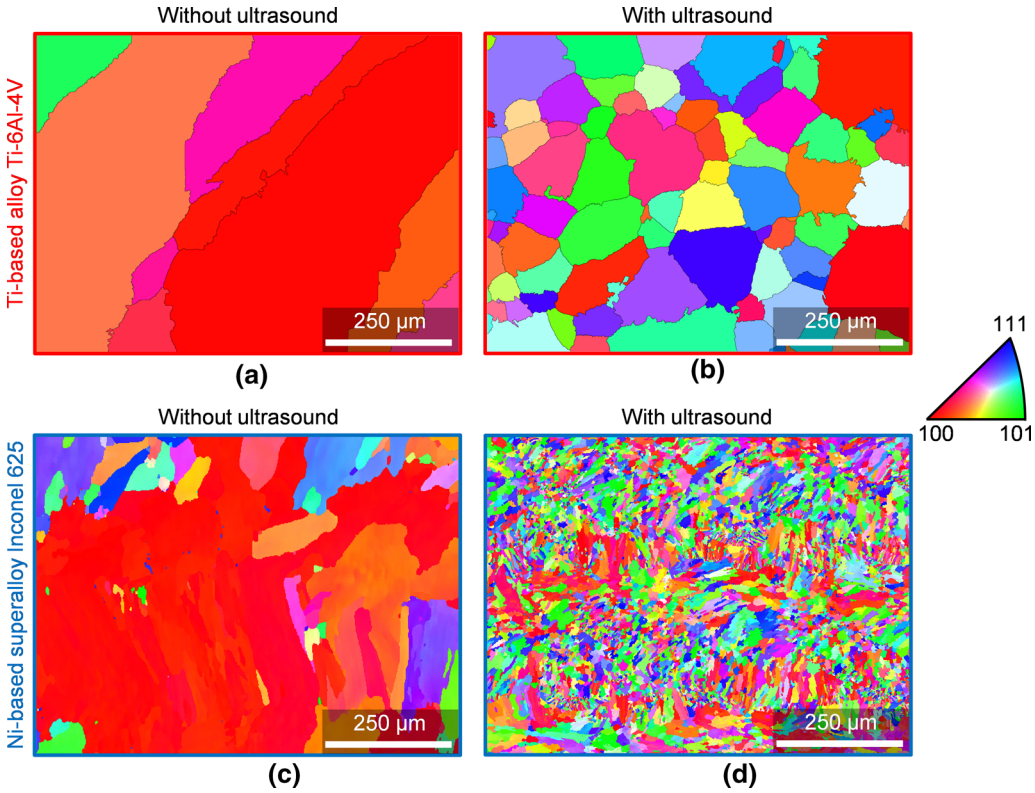


Fig. 7—Grain refinement by high-intensity ultrasound during AM by L-DED. (*a*, *b*) EBSD images of prior $\beta$-Ti grains in Ti-6Al-4V samples (a) without and (b) with ultrasound; (*c*, *d*) EBSD images of $\gamma$-Ni grains in Inconel 625 samples (c) without and (d) with ultrasound. Reprinted from Ref. [178] under the terms of the Creative Commons Attribution 4.0 International (CC BY 4.0) license.

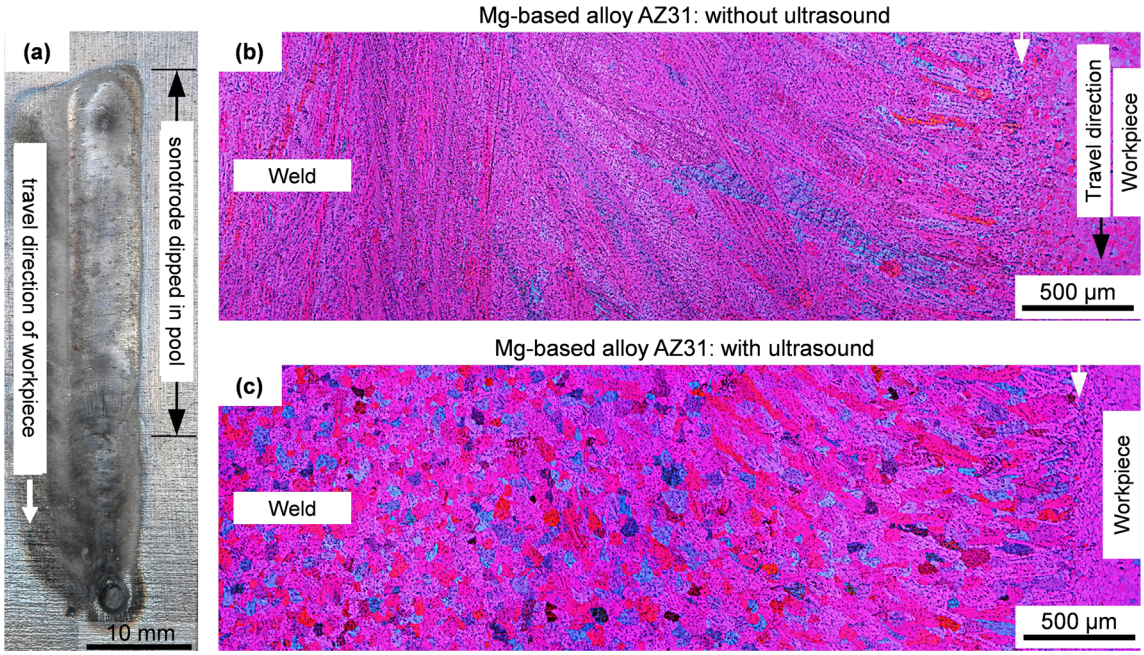


Fig. 8—Grain refinement of Mg-based alloy AZ31 welds by high-intensity ultrasound. (*a*) A weld treated with ultrasound by pushing an ultrasound sonotrode into the melt pool; (*b*, *c*) Polarized light microscopy images of samples (b) without and (c) with ultrasound (frequency: 20 kHz, ultrasound amplitude: 26.44 $\mu$m). Coarse columnar grains are converted to fine (46 $\mu$m) equiaxed grains with the application of ultrasound. Reprinted from Ref. [163] with permission from Elsevier.

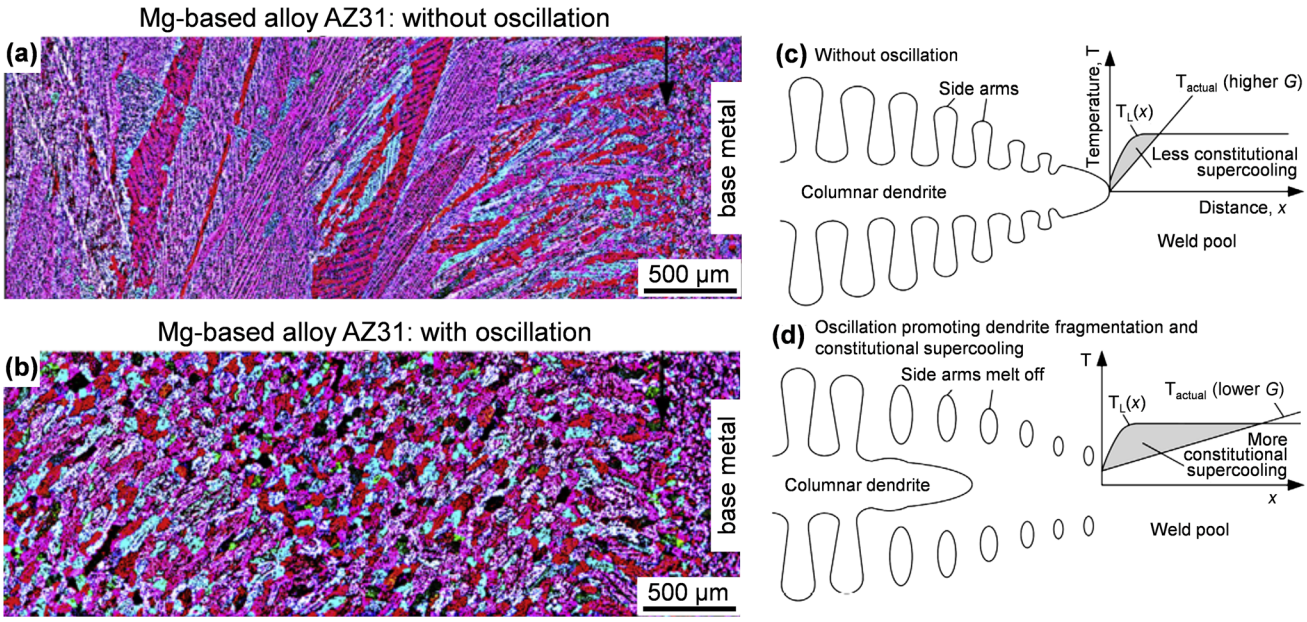


Fig. 9—Grain refinement of Mg-based alloy AZ31 welds by heat source oscillation. (*a*, *b*) Polarized light microscopy images of samples (a) without and (b) with oscillation (frequency: 1 Hz, amplitude: 2 mm); (*c*) The columnar grains in (a) are attributed to the small constitutional supercooling zone formed with a high *G*; (*d*) Arc oscillation promotes (i) dendrite grain fragmentation through reheating and (ii) an enlarged constitutional supercooling zone by reducing *G*. This ensures the survival and further growth of fragments into the equiaxed grains in (b). Reprinted from Ref. [169] with permission from Elsevier.

interest in the development of strategies for incorporating ultrasound into AM systems.

Oscillating the heat source in a controlled manner may also stimulate grain refinement during AM, as the technique has in welding. The energy source can be oscillated by exerting an alternating electric field near the energy source. Oscillation during welding generally occurs at frequencies of ~ 20 Hz and amplitudes of ~ 1 to 2 mm in either transverse, circular, or longitudinal patterns.[165] Figures 9(a) and (b) show grain refinement in Mg-based alloy AZ31 welds by transverse oscillation.[169] Comparing to Figure 8 (grain refinement of the same alloy by ultrasound), it is revealed that the grain-refining potency of ultrasound and oscillation are similar.

Yuan *et al.*[169] investigated the mechanism of grain refinement in transverse oscillated Mg-based alloy welds using the overlapping welding method (as described in Reference [182]) and cooling curve analyses. The results revealed that arc oscillation reheats the $S/L$ interface during solidification, thereby promoting fragmentation of dendrite arms. Additionally, melt stirring by induced flows contributes to a lowered $G$, ensuring the survival and growth of the dendrite fragments into equiaxed grains. The grain refinement mechanism of oscillation is summarized in Figures 9(c) and (d).[169] The results of Yuan *et al.*[169] are consistent with the numerical simulations of an independent study, which suggested that dendrite fragmentation is the major mechanism for oscillation-driven grain refinement of Ni-based alloy welds.[167]

To the authors' knowledge, only two studies have reported oscillating the heat source during AM, although the structural changes appeared to be negligible.[183,184] Clearly, gaps in achieving grain refinement during AM by heat source oscillation can provide opportunities for further research.

Alternatively, the energy source may be manipulated to produce grain refinement by pulsing from high energy to low energy at regular intervals (typically at a frequency between 6 and 20 Hz), as proven during welding of Al-, Fe- and Ti-based alloys.[166,170] In terms of AM, there has been some application of beam pulsing (including tungsten arc (5-25 Hz),[171] plasma arc (70 Hz),[174,175] and laser beam (10 Hz)[173]) to titanium alloy Ti-6Al4V, but in each case the technique showed little influence on the prior $\beta$-Ti grain size.[171,173–175] Similar results have been reported for Ni-based alloy fabricated by pulsed (6.25-50 Hz) L-DED.[185] On the other hand, in a different study focused on EB-PBF of Ni-based superalloy Inconel 718, pulsing the beam in combination with a novel spot melting strategy promoted the CET.[58,186] Hence, it is likely that opportunities exist for grain refinement by heat source pulsing, provided certain conditions are met.

## V. FUTURE APPROACHES TO FURTHER IMPROVING GRAIN REFINEMENT IN AM

The main factors of importance arising from this review are the same factors that are important for all casting processes[5]: the growth restricting ability of the alloying elements and impurities; the nucleation potency of the native or deliberately added nucleant particles; and the casting conditions. A further factor that needs to be considered is the thermal properties of the alloy system such as thermal conductivity and heat capacity.

Recent research[26] shows that these properties affect the rate of latent heat release (recalescence) and cooling rate and in turn the thermal gradient during solidification.

The role of solute and the nucleating particles are well established and are key factors in the determination of grain size by the Interdependence Model. However, the actual solidification conditions during AM are complicated and the mechanisms involved need to be simplified to be able to optimize the process for producing a fine grain size for individual AM processing routes and alloy systems. In this section, we consider the individual melt pool, first quiescently and then dynamically, and finally within the context of the layer building process.

In the case of the individual melt pool, the main difference between many commercial solidification processes and AM is the very high thermal gradients and cooling rates. From a theoretical perspective, a number of factors are becoming clearer. Firstly, the high thermal gradients reduce the amount of CS in front of the interface, which increases the propensity to form columnar grains.[187] On the other hand, there appear to be other effects that refine the microstructure such as the high growth velocities reducing the size of the NFZ, and more importantly increasing the amount of thermal undercooling facilitating nucleation on less potent particles than would be typically the case for casting operations.[29,67] These are the factors that affect the *G*-*V* diagrams that are often used to predict grain morphologies formed during welding and other solidification processes, and increasingly in AM.

The role of cooling rate and thermal gradient on grain size has been evaluated by a number of researchers.[24,54] In particular, Xu *et al.*[24] characterized a grain growing in a thermal gradient in which they defined an inhibited nucleation zone (similar to the NFZ), but also correctly noted that there will be an inhibited zone at a further distance from the interface where once again the undercooling will not be sufficient for nucleation, as shown in Figures 10(a) and (b). However, given the progression of the zone through the melt, nucleation will occur once the region of high undercooling reaches the nucleating substrates.

This understanding of grain refinement points to some potential differences in strategy for obtaining a fine equiaxed grain size in AM. Having sufficient solute available is still critically important, but once a fine grain structure is achieved it appears that the role of solute is less important than the role of the thermal undercooling and the density of nucleant particles. In other words, high potency nucleating substrates appear to be less important than having a high number density of substrates. This suggests that nanoparticles, which are generally considered less effective at nucleating a grain, are more effective nucleants during AM. This has

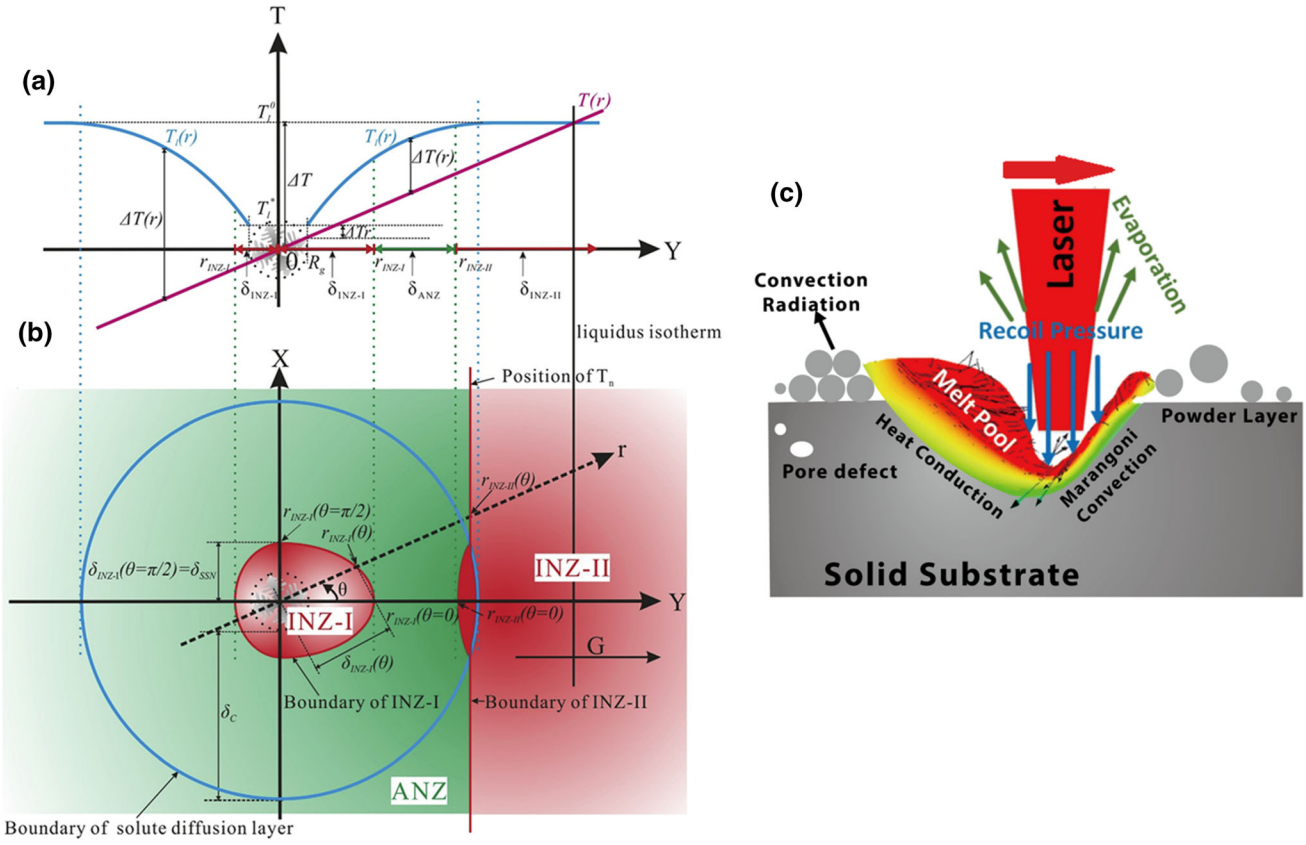


Fig. 10—(*a*) Schematic diagram of the influence of the thermal gradient on the nucleation of new grains around one single grain; (*b*) 2D diagram of the inhibited nucleation zone (INZ), active nucleation zone (ANZ), and the corresponding boundary around one grain, adapted from Ref. [24] with permission from Elsevier; (*c*) A schematic diagram of flow behavior in the molten pool, adapted from Ref. [188] with permission from Springer Nature.

already been exploited in some systems (*e.g.*, Martin *et al.*[106]). It would also suggest that substrates with less effective lattice matching may be useful for AM processes similar to oxides in high pressure die casting.[19] As mentioned above, the thermal properties of the melt and the solid during re-melting and solidification of layers can have a significant effect on recalescence and consequently cooling rate and thermal gradient. A better understanding and quantification of the effect of these properties will allow better comparison of AM process methods and optimization of processing parameters to maximize the number of nucleation events.

Manipulating the conditions in the melt pool is also critically important, which has been shown by the success of some mechanical grain refinement methods such as ultrasonics and arc oscillation, which are designed to interrupt the fluid dynamics of the melt pool and generate further grains (Figure 10(c)). In the case of UST, depending upon the processing parameters, acoustic streaming can reduce the thermal gradient enhancing nucleation of equiaxed grains.[20] It is also known that affecting the Marangoni currents by controlling the energy density by moving into keyhole mode can lead to substantial grain refinement compared to conduction mode.[189] Understanding the effect of process parameters on the melt pool fluid dynamics can possibly affect grain multiplication through fragmentation and grain survival as nucleated grains may be swept into the center of the excessively hot melt pool leading them to re-melt.

Further complicating the AM process is the highly dynamic environment in which manufacturing occurs. It has been noted that in PBF technologies, the powder particles are rapidly spread across the powder bed, and that there can be inhomogeneous melting along the laser track.[71,190] It is unclear how effects such as these may affect the final grain morphology, but are likely to have an effect.

Tracks are placed next to each other and layers are placed on top of the previous layer. While this can lead to the formation of columnar grains through epitaxial growth, it could also be a possibility for assisting refinement, particularly if fragments of the previously melted layer can be separated from the layer to grow in the melt. Furthermore, it may be that eutectic particles or intermetallics that are not normally formed at temperatures above the primary phase can be available long enough before melting to contribute to further nucleation of the primary phase. Clearly, there are a number of avenues for promoting grain refinement that are still available for investigation by researchers that benefit from the highly dynamic conditions in AM.

## VI. CONCLUSIONS

AM processes typically lead to columnar grain structures. This is mainly attributed to the high thermal gradients reducing or eliminating the CS zone in front of the interface, and the use of alloys typically designed for wrought manufacturing with low alloy contents, or with alloying elements that contribute little to generating CS. However, very fine equiaxed grains can be obtained in AM metal alloys. This can be achieved by choosing alloys with enough solute to generate sufficient CS, although once a fine grain size is achieved the role of solute is less pronounced than in casting. Furthermore, the very high cooling rates associated with all AM processes can generate a large amount of thermal undercooling, which in turn can facilitate much more nucleation on lower potency substrates. Both of these factors lead to a finer grain size. Also, the high growth rate leads to a reduction in the nucleation-free or nucleation-inhibited zone. Mechanical means of grain refinement such as ultrasound can also be very effective. The highly dynamic track-by-track and layer-by-layer process of AM provides a number of opportunities for using non-equilibrium approaches to grain refine alloys.

## ACKNOWLEDGMENTS

The authors would like to acknowledge the Australian Research Council (ARC) for their financial support [Grant Numbers DP140100702, DP160100560 and DE160100260] and through the ARC Industrial Training Centre for Lightweight Automotive Structures (ATLAS - IC160100032). M.J. Benoit would like to acknowledge the financial support of the Banting Postdoctoral Fellowship program.

## ABBREVIATIONS

| | |
|---|---|
| AM | Additive manufacturing |
| ANZ | Active nucleation zone |
| CET | Columnar to equiaxed transition |
| CS | Constitutional supercooling |
| EB-PBF | Electron beam powder bed fusion |
| EBSD | Electron backscatter diffraction |
| INZ | Inhibited nucleation zone |
| L-DED | Laser directed energy deposition |
| L-PBF | Laser powder bed fusion |
| LMD | Laser metal deposition |
| NFZ | Nucleation free zone |
| PBF | Powder bed fusion |
| SLM | Selective laser melting |
| WAAM | Wire arc additive manufacturing |

## REFERENCES

1. I. Gibson, D.W. Rosen, and B. Stucker: *Additive Manufacturing Technologies*, Springer, Berlin, 2014.
2. Y. Kok, X.P. Tan, P. Wang, M.L.S. Nai, N.H. Loh, E. Liu, and S.B. Tor: *Mater. Des.*, 2018, vol. 139, pp. 565–86.
3. D.H. StJohn, M. Qian, M.A. Easton, and P. Cao: *Acta Mater.*, 2011, vol. 59, pp. 4907–21.
4. W.C. Winegard and B. Chalmers: *Trans. Am. Soc. Met.*, 1954, vol. 46, pp. 1214–24.
5. M.A. Easton and D.H. StJohn: *Acta Mater.*, 2001, vol. 49, pp. 1867–78.
6. M.X. Zhang, P.M. Kelly, M.A. Easton, and J.A. Taylor: *Acta Mater.*, 2005, vol. 53, pp. 1427–38.

7. J.C. Hunt and B.F. Kiker: *Econ. Educ. Rev.*, 1984, vol. 3, pp. 75–83.
8. M. Gäumann, R. Trivedi, and W. Kurz: *Mater. Sci. Eng., A*, 1997, vols. 226–228, pp. 763–69.
9. M. Qian, P. Cao, M.A. Easton, S.D. McDonald, and D.H. St John: *Acta Mater.*, 2010, vol. 58, pp. 3262–70.
10. D. Shu, B. Sun, J. Mi, and P.S. Grant: *Acta Mater.*, 2011, vol. 59, pp. 2135–44.
11. Q. Du and Y. Li: *Acta Mater.*, 2014, vol. 71, pp. 380–89.
12. A.L. Greer, A.M. Bunn, A. Tronche, P.V. Evans, and D.J. Bristow: *Acta Mater.*, 2000, vol. 48, pp. 2823–35.
13. Y. Jia, D. Wang, Y. Fu, A. Dong, G. Zhu, D. Shu, and B. Sun: *Metall. Mater. Trans. A*, 2019, vol. 50A, pp. 1795–1804.
14. A. Lui, P.S. Grant, I.C. Stone, and K.A.Q. O'Reilly: *Metall. Mater. Trans. A*, 2019, vol. 50A, pp. 5242–52.
15. Y. Li, Z.R. Zhang, Z.Y. Zhao, H.X. Li, L. Katgerman, J.S. Zhang and L.Z. Zhuang: *Metall. Mater. Trans. A*, 2019, pp. 1–14.
16. P.M. Kelly and M.X. Zhang: *Metall. Mater. Trans. A*, 2006, vol. 37, pp. 833–39.
17. D. Qiu, M.X. Zhang, J.A. Taylor, and P.M. Kelly: *Acta Mater.*, 2009, vol. 57, pp. 3052–59.
18. M.X. Zhang, P.M. Kelly, M. Qian, and J.A. Taylor: *Acta Mater.*, 2005, vol. 53, pp. 3261–70.
19. Z. Fan: *Metall. Mater. Trans. A*, 2013, vol. 44A, pp. 1409–18.
20. D.H. StJohn, A. Prasad, M.A. Easton, and M. Qian: *Metall. Mater. Trans. A*, 2015, vol. 46A, pp. 4868–85.
21. M.A. Easton, M. Qian, A. Prasad, and D.H. St John: *Curr. Opin. Solid State Mater. Sci.*, 2016, vol. 20, pp. 13–24.
22. N. Balasubramani, D. StJohn, M. Dargusch, and G. Wang: *Mater.*, 2019, vol. 12, p. 3187.
23. E. Karakulak: *J. Magn. Alloys*, 2019.
24. Y. Xu, D. Casari, R.H. Mathiesen, and Y. Li: *Acta Mater.*, 2018, vol. 149, pp. 312–25.
25. D. H. StJohn, S. D. McDonald, M. J. Bermingham, S. Mereddy, A. Prasad and M. Dargusch: *Key Engineering Materials*, Trans Tech Publ., 2018, pp 155–64.
26. M.J. Bermingham, D.H. StJohn, J. Krynen, S. Tedman-Jones, and M.S. Dargusch: *Acta Mater.*, 2019, vol. 168, pp. 261–74.
27. W. Xu, E.W. Lui, A. Pateras, M. Qian, and M. Brandt: *Acta Mater.*, 2017, vol. 125, pp. 390–400.
28. G.L. Knapp, N. Raghavan, A. Plotkowski, and T. DebRoy: *Additive Manuf.*, 2019, vol. 25, pp. 511–21.
29. A. Prasad, L. Yuan, P. Lee, M. Patel, D. Qiu, M. Easton and D. St John: *Acta Mater.*, 2020, https://doi.org/10.1016/j.actamat.2020.05.012.
30. H.B. Dong and P.D. Lee: *Acta Mater.*, 2005, vol. 53, pp. 659–68.
31. T.E. Quested and A.L. Greer: *Acta Mater.*, 2005, vol. 53, pp. 4643–53.
32. T.S. Srivatsan and T.S. Sudarshan: *Additive Manufacturing: Innovations, Advances, and Applications*, CRC Press, Boca Raton, 2015.
33. D. Gu: *Laser Additive Manufacturing of High-Performance Materials*, Springer, Berlin, 2015.
34. M.L. Griffith, M.E. Schlienger, L.D. Harwell, M.S. Oliver, M.D. Baldwin, M.T. Ensz, M. Essien, J. Brooks, C.V. Robino, J.E. Smugeresky, W.H. Hofmeister, M.J. Wert, and D.V. Nelson: *Mater. Des.*, 1999, vol. 20, pp. 107–13.
35. J.W. Elmer, S.M. Allen, and T.W. Eagar: *Metall. Trans. A*, 1989, vol. 20A, pp. 2117–31.
36. J. Mazumder, In *International Congress on Applications of Lasers & Electro-Optics* (2003).
37. J. Mazumder, A. Schifferer, and J. Choi: *MRS Proc.*, 1998, vol. 542, p. 51.
38. W. Hofmeister and M. Griffith: *JOM*, 2001, vol. 53, pp. 30–34.
39. P.A. Kobryn and S.L. Semiatin: *J. Mater. Process. Technol.*, 2003, vol. 135, pp. 330–39.
40. M. Doubenskaia, P. Bertrand, and I. Smurov: *Surf. Coat. Technol.*, 2006, vol. 201, pp. 1955–61.
41. S.S. Al-Bermani, M.L. Blackmore, W. Zhang, and I. Todd: *Metall. Mater. Trans. A*, 2010, vol. 41A, pp. 3422–34.
42. M.H. Farshidianfar, A. Khajepour, and A.P. Gerlich: *J. Mater. Process. Technol.*, 2016, vol. 231, pp. 468–78.
43. T. Vilaro, C. Colin, and J.D. Bartout: *Metall. Mater. Trans. A*, 2011, vol. 42A, pp. 3190–99.
44. U.S. Bertoli, G. Guss, S. Wu, M.J. Matthews, and J.M. Schoenung: *Mater. Des.*, 2017, vol. 135, pp. 385–96.
45. P.A. Hooper: *Additive Manuf.*, 2018, vol. 22, pp. 548–59.
46. S. Sun, M. Brandt and M. Easton: *Laser Additive Manuf.: Mat., Des., Technol. App.*, 2017, pp 55–77.
47. J.J. Blecher, T.A. Palmer, and T. DebRoy: *Metall. Mater. Trans. A*, 2014, vol. 45A, pp. 2142–51.
48. W. Ou, T. Mukherjee, G.L. Knapp, Y. Wei, and T. DebRoy: *Int. J. Heat Mass Transfer*, 2018, vol. 127, pp. 1084–94.
49. L. Qian, J. Mei, J. Liang, and X. Wu: *Mater. Sci. Technol.*, 2005, vol. 21, pp. 597–605.
50. R. Rai, J.W. Elmer, T.A. Palmer, and T. DebRoy: *J. Phys. D Appl. Phys.*, 2007, vol. 40, pp. 5753–66.
51. P. Yuan and D. Gu: *J. Phys. D Appl. Phys.*, 2015, vol. 48, pp. 1–16.
52. S. Gorsse, C. Hutchinson, M. Gouné, and R. Banerjee: *Sci. Technol. Adv. Mater.*, 2017, vol. 18, pp. 584–610.
53. L.E. Murr: *Metall. Microstruct. Anal.*, 2018, vol. 7, pp. 103–32.
54. M. Sun, D. H. St John, M. A. Easton, K. Wang and J. Ni: *Metall. Mater. Trans. A*, 2019.
55. N.J. Harrison, I. Todd, and K. Mumtaz: *Acta Mater.*, 2015, vol. 94, pp. 59–68.
56. J. A. Dantzig and M. Rappaz: *Solidification*, 2nd ed. (EPFL Press, 2016).
57. P. Liu, Z. Wang, Y. Xiao, M.F. Horstemeyer, X. Cui, and L. Chen: *Addit. Manuf.*, 2019, vol. 26, pp. 22–29.
58. N. Raghavan, R. Dehoff, S. Pannala, S. Simunovic, M. Kirka, J. Turner, N. Carlson, and S.S. Babu: *Acta Mater.*, 2016, vol. 112, pp. 303–14.
59. A. Hadadzadeh, B.S. Amirkhiz, J. Li, and M. Mohammadi: *Additive Manuf.*, 2018, vol. 23, pp. 121–31.
60. W. Kurz and D.J. Fisher: *Fundamentals of Solidification*, Trans Tech Publications Limited, 1998.
61. W. Kurz and R. Trivedi: *Mater. Sci. Eng., A*, 1994, vols. 179–180, pp. 46–51.
62. J.D. Hunt: *Mater. Sci. Eng.*, 1984, vol. 65, pp. 75–83.
63. A.L. Greer: *Phil. Trans: Math. Phys. Eng. Sci*, 2003, vol. 361, pp. 479–95.
64. W. Kurz, C. Bezençon, and M. Gäumann: *Sci. Technol. Adv. Mater.*, 2001, vol. 2, pp. 185–91.
65. J. Wang, X. Lin, J. Wang, H. Yang, Y. Zhou, C. Wang, Q. Li, and W. Huang: *J. Alloys Compd.*, 2018, vol. 768, pp. 97–113.
66. M. Haines, A. Plotkowski, C.L. Frederick, E.J. Schwalbach, and S.S. Babu: *Comput. Mater. Sci.*, 2018, vol. 155, pp. 340–49.
67. M.N. Patel, D. Qiu, G. Wang, M.A. Gibson, A. Prasad, D.H. StJohn, and M.A. Easton: *Scripta Mater.*, 2020, vol. 178, pp. 447–51.
68. D. Zhang, D. Qiu, M.A. Gibson, Y. Zheng, H.L. Fraser, D.H. StJohn, and M.A. Easton: *Nature*, 2019, vol. 576, pp. 91–95.
69. P.C. Collins, D.A. Brice, P. Samimi, I. Ghamarian, and H.L. Fraser: *Annu. Rev. Mater. Res.*, 2016, vol. 46, pp. 63–91.
70. F. Yan, W. Xiong, and E.J. Faierson: *Mater.*, 2017, vol. 10, pp. 1–11.
71. C. Zhao, K. Fezzaa, R.W. Cunningham, H. Wen, F. De Carlo, L. Chen, A.D. Rollett, and T. Sun: *Sci. Rep.*, 2017, vol. 7, pp. 1–11.
72. R. Boyer, G. Welsch, and E.W. Collings: *Materials Properties Handbook: Titanium Alloys*, ASM International, Materials Park, OH, 1994.
73. M.J. Bermingham, S.D. McDonald, M.S. Dargusch, and D.H. St John: *J. Mater. Res.*, 2008, vol. 23, pp. 98–104.
74. G.V. Samsonov, V.A. Kashchuk, and A.I. Cherkashin: *Metallovedenie i Termicheskaya Obrabotka Metallov*, 1970, vol. 11, pp. 30–31.
75. M.J. Bermingham, S.D. McDonald, D.H. StJohn, and M.S. Dargusch: *J. Alloys Compd.*, 2009, vol. 481, pp. L20–L23.
76. H. Okamoto: *J. Phase Equilib.*, 2000, vol. 21, p. 311.
77. H. Okamoto: *Desk Handbook Phase Diagrams for Binary Alloys*, ASM International, Materials Park, OH, 2000.
78. M.J. Bermingham, S.D. McDonald, A.J. Buddery, D.H. StJohn, and M.S. Dargusch: *Mater. Sci. Eng., C*, 2011, vol. 31, pp. 1520–25.

79. M.Y. Mendoza, P. Samimi, D.A. Brice, B.W. Martin, M.R. Rolchigo, R. LeSar and P.C. Collins: *Metall. Mater. Trans. A* 2017, pp. 1–12.
80. S. Mereddy, M.J. Bermingham, D. Kent, A. Dehghan-Manshadi, D.H. StJohn, and M.S. Dargusch: *JOM*, 2018, vol. 70, pp. 1670–76.
81. M.J. Bermingham, D. Kent, H. Zhan, D.H. StJohn, and M.S. Dargusch: *Acta Mater.*, 2015, vol. 91, pp. 289–303.
82. M.J. Bermingham, S.D. McDonald, and M.S. Dargusch: *Mater. Sci. Eng., A*, 2018, vol. 719, pp. 1–11.
83. S.A. Mantri, T. Alam, D. Choudhuri, C.J. Yannetta, C.V. Mikler, P.C. Collins, and R. Banerjee: *J. Mater. Sci.*, 2017, vol. 52, pp. 12455–466.
84. R.A. Rahman Rashid, S. Palanisamy, H. Attar, M. Bermingham and M.S. Dargusch: *J. Manuf. Processes* 2018, vol. 35, pp. 651–656.
85. A. Xue, X. Lin, L. Wang, J. Wang, and W. Huang: *Mater. Des.*, 2019, vol. 181, p. 107943.
86. K. Zhang, X. Tian, M. Bermingham, J. Rao, Q. Jia, Y. Zhu, X. Wu, S. Cao, and A. Huang: *Mater. Des.*, 2019, vol. 184, p. 108191.
87. R. Banerjee, P.C. Collins, A. Genç, and H.L. Fraser: *Mater. Sci. Eng. A*, 2003, vol. 358, pp. 343–49.
88. S. Mereddy, M.J. Bermingham, D.H. StJohn, and M.S. Dargusch: *J. Alloys Compd.*, 2017, vol. 695, pp. 2097–2103.
89. X. Lin, T.M. Yue, H.O. Yang, and W.D. Huang: *Metall. Mater. Trans. A*, 2007, vol. 38, pp. 127–37.
90. M.J. Bermingham, S.D. McDonald, D.H. StJohn, and M.S. Dargusch: *Philos. Mag.*, 2010, vol. 90, pp. 699–715.
91. S.N. Tedman-Jones, M.J. Bermingham, S.D. McDonald, D.H. StJohn, and M.S. Dargusch: *J. Alloys Compd.*, 2020, vol. 818, p. 153353.
92. S.N. Tedman-Jones, S.D. McDonald, M.J. Bermingham, D.H. StJohn, and M.S. Dargusch: *J. Alloys Compd.*, 2019, vol. 794, pp. 268–84.
93. D. Qiu, D. Zhang, M.A. Easton, D.H. St John and M.A. Gibson: *Metall. Mater. Trans. A*, 2018, vol. 49, pp. 1444–49.
94. T. Wang, Y.Y. Zhu, S.Q. Zhang, H.B. Tang, and H.M. Wang: *J. Alloys Compd.*, 2015, vol. 632, pp. 505–13.
95. Q. Zhang, J. Chen, X. Lin, H. Tan, and W.D. Huang: *J. Mater. Process. Technol.*, 2016, vol. 238, pp. 202–11.
96. F.A. Crossley: ed. USPTO (Lockheed Missiles & Space Company, Inc.: USA, 1983).
97. F.A. Crossley: *SAMPE J.* 1986, vol. 22, pp. 31–34.
98. F. Wang, Z.L. Liu, D. Qiu, J.A. Taylor, M.A. Easton, and M.X. Zhang: *Acta Mater.*, 2013, vol. 61, pp. 360–70.
99. P. Barriobero-Vila, J. Gussone, A. Stark, N. Schell, J. Haubrich, and G. Requena: *Nat. Commun.*, 2018, vol. 9, p. 3426.
100. Y.S. Tian, C.Z. Chen, L.X. Chen and Q.H. Huo: *Scripta Mater.*, 2006, vol. 54.
101. R.P. Simpson: *Weld. J.*, 1977, vol. 56, pp. 67–77.
102. M.C. Nordin, G.R. Edwards, and D.L. Olson: *Weld. J.*, 1987, vol. 66, pp. 342–52.
103. M.S. Misra: *Martin Marietta Aerospace*, Denver, United States, 1983.
104. D.D. Gu, W. Meiners, K. Wissenbach, and R. Poprawe: *Int. Mater. Rev.*, 2012, vol. 57, pp. 133–64.
105. K. Schmidtke, F. Palm, A. Hawkins, and C. Emmelmann: *Phys. Proc.*, 2011, vol. 12, pp. 369–74.
106. J.H. Martin, B.D. Yahata, J.M. Hundley, J.A. Mayer, T.A. Schaedler, and T.M. Pollock: *Nature*, 2017, vol. 549, pp. 365–69.
107. E.O. Olakanmi, R.F. Cochrane, and K.W. Dalgarno: *Prog. Mater Sci.*, 2015, vol. 74, pp. 401–77.
108. D. Zhang, S. Sun, D. Qiu, M.A. Gibson, M.S. Dargusch, M. Brandt, M. Qian, and M. Easton: *Adv. Eng. Mater.*, 2018, vol. 20, p. 1700952.
109. E. Louvis, P. Fox, and C.J. Sutcliffe: *J. Mater. Process. Technol.*, 2011, vol. 211, pp. 275–84.
110. P. Wang, H.C. Li, K.G. Prashanth, J. Eckert, and S. Scudino: *J. Alloys Compd.*, 2017, vol. 707, pp. 287–90.
111. T. Qi, H. Zhu, H. Zhang, J. Yin, L. Ke, and X. Zeng: *Mater. Des.*, 2017, vol. 135, pp. 257–66.
112. N. Kaufmann, M. Imran, T.M. Wischeropp, C. Emmelmann, S. Siddique, and F. Walther: *Phys. Procedia*, 2016, vol. 83, pp. 918–26.
113. J. Gu, J. Bai, J. Ding, S. Williams, L. Wang, and K. Liu: *J. Mater. Process. Technol.*, 2018, vol. 262, pp. 210–20.
114. Nesma.T. Aboulkhair, Marco. Simonelli, Luke. Parry, Ian. Ashcroft, Christopher. Tuck, and Richard. Hague: *Prog. Mater Sci.*, 2019, vol. 106, p. 100578.
115. Maria.L. Montero-Sistiaga, Raya. Mertens, Bey. Vrancken, Xiebin. Wang, Brecht. Van Hooreweder, Jean.-Pierre. Kruth, and Jan. Van Humbeeck: *J. Mater. Process. Technol.*, 2016, vol. 238, pp. 437–45.
116. R. Casati, M. Coduri, M. Riccio, A. Rizzi, and M. Vedani: *J. Alloys Compd.*, 2019, vol. 801, pp. 243–53.
117. N. Takata, H. Kodaira, K. Sekizawa, A. Suzuki, and M. Kobashi: *Mater. Sci. Eng., A*, 2017, vol. 704, pp. 218–28.
118. E. Brandl, U. Heckenberger, V. Holzinger, and D. Buchbinder: *Mater. Des.*, 2012, vol. 34, pp. 159–69.
119. Y.C. Lee, A.K. Dahle, D.H. StJohn, and J.E.C. Hutt: *Mater. Sci. Eng., A*, 1999, vol. 259, pp. 43–52.
120. X. Liu, C. Zhao, X. Zhou, Z. Shen, and W. Liu: *Mater. Des.*, 2019, vol. 168, p. 107677.
121. X.J. Nie, H. Zhang, H.H. Zhu, Z.H. Hu, L.D. Ke, and X.Y. Zeng: *J. Alloys Compd.*, 2018, vol. 764, pp. 977–86.
122. H. Zhang, H. Zhu, X. Nie, J. Yin, H. Zhiheng, and X. Zeng: *Scripta Mater.*, 2017, vol. 134, pp. 6–10.
123. Z. Fan, F. Gao, L. Zhou, and S.Z. Lu: *Acta Mater.*, 2018, vol. 152, pp. 248–57.
124. Y.K. Xiao, Z.Y. Bian, Y. Wu, G. Ji, Y.Q. Li, M.J. Li, Q. Lian, Z. Chen, A. Addad, and H.W. Wang: *J. Alloys Compd.*, 2019, vol. 798, pp. 644–55.
125. D. Carluccio, M.J. Bermingham, Y. Zhang, D.H. StJohn, K. Yang, P.A. Rometsch, X. Wu, and M.S. Dargusch: *J. Manuf. Processes*, 2018, vol. 35, pp. 715–20.
126. P. Wang, C. Gammer, F. Brenne, T. Niendorf, J. Eckert, and S. Scudino: *Compos. B Eng.*, 2018, vol. 147, pp. 162–68.
127. X. Wen, Q. Wang, Q. Mu, N. Kang, S. Sui, H. Yang, X. Lin, and W. Huang: *Mater. Sci. Eng., A*, 2019, vol. 745, pp. 319–25.
128. Q. Tan, J. Zhang, N. Mo, Z. Fan, Y. Yin, M. Bermingham, Y. Liu, H. Huang and Ming-Xing Zhang: *Additive Manuf.*, 2020, p. 101034.
129. M.A. Easton and D.H. StJohn: *Metall. Mater. Trans. A*, 2005, vol. 36A, pp. 1911–20.
130. D.G. McCartney: *Int. Mater. Rev.*, 1989, vol. 34, pp. 247–60.
131. M. Johnsson and L. Bäckerud: *Zeitschrift fuer Metallkunde/Materials Research and Advanced Techniques*, 1996, vol. 87, pp. 216–20.
132. Q. Jia, P. Rometsch, P. Kürnsteiner, Q. Chao, A. Huang, M. Weyland, L. Bourgeois, and W. Xinhua: *Acta Mater.*, 2019, vol. 171, pp. 108–18.
133. F. Wang, D. Qiu, Z.L. Liu, J.A. Taylor, M.A. Easton, and M.X. Zhang: *Acta Mater.*, 2013, vol. 61, pp. 5636–45.
134. S. Griffiths, M.D. Rossell, J. Croteau, N.Q. Vo, D.C. Dunand, and C. Leinenbach: *Mater. Charact.*, 2018, vol. 143, pp. 34–42.
135. J.R. Croteau, S. Griffiths, M.D. Rossell, C. Leinenbach, C. Kenel, V. Jansen, D.N. Seidman, D.C. Dunand, and N.Q. Vo: *Acta Mater.*, 2018, vol. 153, pp. 35–44.
136. K.V. Yang, Y.J. Shi, F. Palm, X.H. Wu, and P. Rometsch: *Scripta Mater.*, 2018, vol. 145, pp. 113–17.
137. Y. Shi, P. Rometsch, K. Yang, F. Palm, and X. Wu: *Mater. Lett.*, 2017, vol. 196, pp. 347–50.
138. A.B. Spierings, K. Dawson, M. Voegtlin, F. Palm, and P.J. Uggowitzer: *CIRP Ann.*, 2016, vol. 65, pp. 213–16.
139. Y. Shi, K. Yang, S.K. Kairy, F. Palm, X. Wu, and P.A. Rometsch: *Mater. Sci. Eng., A*, 2018, vol. 732, pp. 41–52.
140. L. Zhou, H. Pan, H. Hyer, S. Park, Y. Bai, B. McWilliams, K. Cho, and Y. Sohn: *Scripta Mater.*, 2019, vol. 158, pp. 24–28.
141. S. Kou: *Weld. J.*, 2015, vol. 94, pp. 374s–388s.
142. X. Chen, J. Li, X. Cheng, H. Wang, and Z. Huang: *Mater. Sci. Eng., A*, 2018, vol. 715, pp. 307–14.
143. X. Ran, D. Liu, J. Li, H. Wang, X. Cheng, J. Zhang, H. Tang, and X. Liu: *Mater. Sci. Eng., A*, 2018, vol. 721, pp. 251–62.
144. F. Zhang, L.E. Levine, A.J. Allen, M.R. Stoudt, G. Lindwall, E.A. Lass, M.E. Williams, Y. Idell, and C.E. Campbell: *Acta Mater.*, 2018, vol. 152, pp. 200–14.
145. S. Sun, Y. Koizumi, S. Kurosu, Y. Li, and A. Chiba: *Acta Mater.*, 2015, vol. 86, pp. 305–18.
146. B. AlMangour, D. Grzesiak, and J. Yang: *Mater. Des.*, 2016, vol. 96, pp. 150–61.

147. B. AlMangour, D. Grzesiak, and J. Yang: *J. Alloys Compd.*, 2017, vol. 728, pp. 424–35.
148. B. Li, B. Qian, Y. Xu, Z. Liu, J. Zhang, and F. Xuan: *Mater. Sci. Eng., A*, 2019, vol. 745, pp. 495–508.
149. I. Ting Ho, Y.-T. Chen, A.-C. Yeh, C.-P. Chen and K.-K. Jen: *Addit. Manuf.*, 2018, vol. 21, pp. 465–71.
150. P.L. Schaffer, A.K. Dahle and J.W. Zindel: *TMS Light Metals*, 2004, pp. 821–26.
151. C. Vives: *Metall. Mater. Trans. B*, 1989, vol. 20B, pp. 623–29.
152. C. Vives: *Metall. Mater. Trans. B*, 1989, vol. 20B, pp. 631–43.
153. S. Ji, Z. Fan, and M.J. Bevis: *Mater. Sci. Eng., A*, 2001, vol. 299, pp. 210–17.
154. T. Campanella, C. Charbon, and M. Rappaz: *Metall. Mater. Trans. A*, 2004, vol. 35A, pp. 3201–10.
155. X. Jian, H. Xu, T.T. Meek, and Q. Han: *Mater. Lett.*, 2005, vol. 59, pp. 190–93.
156. Z. Fan and G. Liu: *Acta Mater.*, 2005, vol. 53, pp. 4345–57.
157. A. Ramirez, M. Qian, B. Davis, and T. Wilks: *Int. J. Cast Met.*, 2009, vol. 22, pp. 260–63.
158. Z. Fan, Y. Wang, M. Xia, and S. Arumuganathar: *Acta Mater.*, 2009, vol. 57, pp. 4891–4901.
159. T.V. Atamanenko, D.G. Eskin, L. Zhang and L. Katgerman: *Metall. Mater. Trans. A*, 2010, vol. 41a, pp. 2056–66.
160. T. Watanabe, S. Ookawara, S. Seki, A. Yanagisawa, and S. Konuma: *Q. J. Jpn. Weld. Soc.*, 2003, vol. 21, pp. 249–55.
161. Y. Cui, C.L. Xu, and Q. Han: *Scripta Mater.*, 2006, vol. 55, pp. 975–78.
162. Y. Cui, C.L. Xu, and Q.Y. Han: *Adv. Eng. Mater.*, 2007, vol. 9, pp. 161–63.
163. T. Yuan, S.D. Kou, and Z. Luo: *Acta Mater.*, 2016, vol. 106, pp. 144–54.
164. R. Thavamani, V. Balusamy, J. Nampoothiri, R. Subramanian and K.R. Ravi: *J. Alloys Compd.*, 2018, vol. 740, pp. 870–78.
165. S. Kou and Y. Le: *Met. Trans. A*, 1985, vol. 16, pp. 1345–52.
166. S.R. Koteswara Rao, G. Madhusudhana Reddy, M. Kamaraj and K. Prasad Rao: *Mater. Sci. Eng. A*, 2005, vol. 404, pp. 227–34.
167. Y.C. Lim, X. Yu, J.H. Cho, J. Sosa, D.F. Farson, S.S. Babu, S. McCracken, and B. Flesner: *Sci. Technol. Weld. Join.*, 2010, vol. 15, pp. 583–89.
168. Y.C. Lim, X. Yu, J.H. Cho, J. Sosa, D.F. Farson, S.S. Babu, S. McCracken, and B. Flesner: *Sci. Technol. Weld. Join.*, 2010, vol. 15, pp. 400–06.
169. T. Yuan, Z. Luo, and S. Kou: *Acta Mater.*, 2016, vol. 116, pp. 166–76.
170. D.W. Becker and C.M. Adams: *Weld. J.*, 1979, vol. 58, pp. 143s–52s.
171. F. Wang, S. Williams, and M. Rush: *Int. J. Adv. Manuf. Tech.*, 2011, vol. 57, pp. 597–603.
172. R.R. Dehoff, M.M. Kirka, W.J. Sames, H. Bilheux, A.S. Tremsin, L.E. Lowe, and S.S. Babu: *Mater. Sci. Technol.*, 2015, vol. 31, pp. 931–38.
173. A.R. Nassar and E.W. Reutzel: *Metall. Mater. Trans. A*, 2015, vol. 46a, pp. 2781–89.
174. J.J. Lin, Y.H. Lv, Y.X. Liu, B.S. Xu, Z. Sun, Z.G. Li, and Y.X. Wu: *Mater. Des.*, 2016, vol. 102, pp. 30–40.
175. J. Lin, Y. Lv, Y. Liu, Z. Sun, K. Wang, Z. Li, Y. Wu, and B. Xu: *J. Mech. Behav. Biomed. Mater.*, 2017, vol. 69, pp. 19–29.
176. M. Qian, A. Ramirez, and A. Das: *J. Cryst. Growth*, 2009, vol. 311, pp. 3708–15.
177. G.I. Eskin and D.G. Eskin: *Ultrasonic Treatment of Light Alloy Melts*, 2nd ed., CRC Press, Boca Raton, 2014.
178. C.J. Todaro, M.A. Easton, D. Qiu, D. Zhang, M.J. Bermingham, E.W. Lui, M. Brandt, D.H. StJohn, and M. Qian: *Nat. Commun.*, 2020, vol. 11, p. 142.
179. Y. Zhang, Y. Guo, Y. Chen, Y. Cao, H. Qi, and S. Yang: *Materials*, 2020, vol. 13 (1), p. 126.
180. D.H. StJohn, M.A. Easton, and M. Qian: *Sol. St. Phen.*, 2008, vols. 141–143, pp. 355–60.
181. G. Wang, Q. Wang, M.A. Easton, M.S. Dargusch, M. Qian, D.G. Eskin, and D.H. StJohn: *Sci. Rep.*, 2017, vol. 7, p. 9729.
182. S. Kou and Y. Le: *Weld. J.*, 1986, vol. 65, pp. 305s–13s.
183. F. Liu, H. Cheng, X. Yu, G. Yang, C. Huang, X. Lin, and J. Chen: *Opt. Laser Technol.*, 2018, vol. 99, pp. 342–50.
184. B. Lu, X. Cui, L. Jiang, E. Liu, D. Zhang, X. Feng, M. Dong, and G. Jin: *Surf. Coat. Technol.*, 2019, vol. 359, pp. 125–31.
185. R.J. Moat, A.J. Pinkerton, L. Li, P.J. Withers, and M. Preuss: *Acta Mater.*, 2009, vol. 57 (4), pp. 1220–29.
186. R.R. Dehoff, M.M. Kirka, F.A. List, K.A. Unocic, and W.J. Sames: *Mater. Sci. Tech.*, 2015, vol. 31 (8), pp. 939–44.
187. A. Prasad, L. Yuan, P.D. Lee, M. Easton, and D. StJohn: *IOP Conf. Series: Mater. Sci. Eng.*, 2016, vol. 117, pp. 1–7.
188. B. Cheng, L. Loeber, H. Willeck, U. Hartel, and C. Tuffile: *J. Mater. Eng. Perform.*, 2019, vol. 28, pp. 6565–78.
189. M. Wahba, M. Mizutani, Y. Kawahito, and S. Katayama: *Sci. Technol. Weld. Join.*, 2010, vol. 15, pp. 559–66.
190. C. Leung, S. Marussi, R.C. Atwood, M. Towrie, P.J. Withers, and P.D. Lee: *Nat. Commun.*, 2018, vol. 9, p. 1355.